RAPID COMMUNICATIONS IN MASS SPECTROMETRY
Rapid Commun. Mass Spectrom. 2001; **15**: 2240–2258

Comparative analysis of glycosylinositol phosphorylceramides from fungi by electrospray tandem mass spectrometry with low-energy collision-induced dissociation of Li^+ adduct ions

Steven B. Levery[1]*, Marcos S. Toledo[2], Anita H. Straus[2] and Helio K. Takahashi[2]

[1]The Complex Carbohydrate Research Center and Department of Biochemistry and Molecular Biology, University of Georgia, 220 Riverbend Road, Athens, GA 30602-4712, USA
[2]Department of Biochemistry, Universidade Federal de São Paulo/Escola Paulista de Medicina, Rua Botucatu 862, 04023-900, São Paulo, SP, Brasil

Received 24 July 2001; Revised 2 October 2001; Accepted 4 October 2001

Glycosylinositol phosphorylceramides (GIPCs) are a class of acidic glycosphingolipids (GSLs) expressed by fungi, plants, and certain parasitic organisms, but not found in cells or tissues of mammals or other higher animals. Recent characterizations of fungal GIPCs point to an emerging diversity which could rival that already known for mammalian GSLs, and which can be expected to present a multitude of challenges for the analytical chemist. Previously, the use of Li^+ cationization, in conjunction with electrospray ionization mass spectrometry (ESI-MS) and low-energy collision-induced dissociation tandem mass spectrometry (ESI-MS/CID-MS), was found to be particularly effective for detailed structural analysis of monohexosylceramides (cerebrosides) from a variety of sources, including fungi, especially minor components present in mixtures at extremely low abundance. In applying Li^+ cationization to characterization of GIPCs, a substantial increase in both sensitivity and fragmentation was observed on collision-induced dissociation of $[M + Li]^+$ versus $[M + Na]^+$ for the same components analyzed under similar conditions, similar to results obtained previously with cerebrosides. Molecular adduct fragmentation patterns were found to be systematic and characteristic for both the glycosylinositol and ceramide moieties with or without phosphate. Interestingly, significant differences were observed in fragmentation patterns when comparing GIPCs having Manα1 → 2 versus Manα1 → 6Ins core linkages. In addition, it was useful to perform tandem product ion scans on primary fragments generated in the orifice region, equivalent to ESI-(CID-MS)^2 mode. Finally, precursor ion scanning from appropriate glycosylinositol phosphate product ions yielded clean molecular ion profiles in the presence of obscuring impurity peaks. The methods were applied to detailed characterization of GIPC fractions of increasing structural complexity from a variety of fungi, including a non-pathogenic Basidiomycete (mushroom), *Agaricus blazei*, and pathogenic Euascomycete species such as *Aspergillus fumigatus*, *Histoplasma capsulatum*, and *Sporothrix schenckii*. The analysis confirmed a remarkable diversity of GIPC structures synthesized by the dimorphic *S. schenckii*, as well as differential expression of both glycosylinositol and ceramide structures in the mycelium and yeast forms of this mycopathogen. Mass spectrometry also established that the ceramides of some *A. fumigatus* GIPC fractions contain very little 2-hydroxylation of the long-chain fatty-*N*-acyl moiety, a feature that is not generally observed with fungal GIPCs.

Sphingolipids, derivatives of the sphingoid bases (i.e., 1,3-dihydroxy-2-amino-substituted long-chain hydrocarbons), comprise a structurally and functionally diverse class of natural products found in cell membrane fractions of all eukaryotes and some bacteria.[1] Among various biological taxa, the pathways for sphingolipid biosynthesis are characterized by both common and distinctive elements, but overall their expression appears to be essential for normal life processes at both the uni- and multicellular levels.[2] In mammals and other animal phyla, 1-*O*-glycosylated sphingolipids (glycosphingolipids, GSLs)[1] are commonly based on diverse extensions of *β-gluco*pyranosyl- or *β-galacto*-pyranosylceramide (*N*-acyl-sphingosine); only one phosphorylated ceramide derivative, sphingomyelin, or choline phosphorylceramide, is found in quantity in any mam-

**Correspondence to*: S. B. Levery, The Complex Carbohydrate Research Center, University of Georgia, 220 Riverbend Road, Athens, GA 30602-4712, USA.
E-mail: leverysb@ccrc.uga.edu

DOI:10.1002/rcm.505

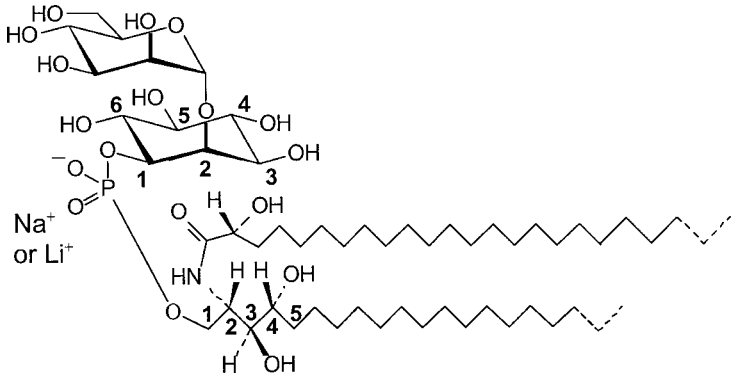

Scheme 1. Representative structure for GIPCs used in this study, with numbering of sphingoid (phytosphingosine) and *myo*-inositol (Ins) residue. Depicted are predominant lipoforms of Manα1 $\rightarrow$ 2InsPCer (Mα2IPC) from *Agaricus blazei*, where sphingoid may be either t18:0 or t20:0, fatty-N-acylation may be either h22:0 or h24:0.

malian tissues. On the other hand, a major subclass of acidic GSLs, the glycosylinositol phosphorylceramides (GIPCs; illustrated in Scheme 1), characterized by interpolation of a *myo*-inositol-1-phosphate (Ins-P-) moiety between glycan and ceramide, is expressed by fungi, plants, and certain parasitic organisms, but is not found in cells or tissues of mammals or other higher animals.[3] Inositol phosphorylceramide (IPC) synthase, which catalyzes the obligatory first step in the biosynthesis of GIPCs,[4–6] is the specific target of several inhibitory drugs which can fatally disrupt fungal cellular processes.[5,7–9] IPC synthase inhibitors are highly toxic to many fungi, including a variety of mycopathogens, but have no effect on mammalian cells which lack this enzyme.[2] IPC synthase inhibitors therefore show considerable promise as antifungal therapeutic agents.[4,10,11] There is thus a growing interest in the structure, biosynthesis, and functional roles of fungal GIPCs. Specific GIPCs also appear to be antigenic in humans, or otherwise interact with the host immune system,[12–15] but detailed knowledge of their structures has for many years been confined to a very few species.[3,5] Nonetheless, recent characterizations of fungal GIPCs point to an emerging diversity which could rival that already known for mammalian GSLs.[16–19]

Understanding the possible roles of GIPCs in fungal cellular function and host-pathogen interactions will be facilitated by the development of routine and sensitive protocols for detailed structural and quantitative analysis of fungal GIPCs, including biosynthetic intermediates and metabolic products which may be present in very low abundance. Such methods will be invaluable for correlating the expression of GIPC structural variants with different species, strains, or culture conditions; and with fungal growth, differentiation, morphogenesis, or pathogenicity; as well as for detection and elucidation of previously unknown structures.

Mass spectrometry has long been a critical tool for structural analysis of GSLs,[20–24] as the glycan moiety is amenable to sequencing by a wide variety of high- and low-energy mass spectrometric techniques. In addition, details about ceramide primary structures, including some that are not easily determined by NMR analysis, are readily available from MS analysis. The use of Li^+ cationization with high-energy collision-induced dissociation (CID) was established for analysis of ceramides and simple glycosphingolipids by Ann and Adams,[25,26] and subsequently applied to characterization of monohexosylceramides (CMHs, also referred to as cerebrosides) from, e.g., fungi, plants, and corals.[27–29] The efficacy of the method was demonstrated at lower collision energies by Olling *et al.*,[30] in a magnetic sector time-of-flight (TOF) hybrid fitted with an electrospray ionization (ESI) source, and applied to more complex glycosphingolipids. Subsequently, Li^+ cationization, in conjunction with low-energy tandem quadrupole ESI-MS/CID-MS, was applied in our laboratory to cerebrosides from a number of different sources, including bovine brain, soybean, and various fungi,[31] with a view towards correlating the appearance of characteristic fragmentation modes, under these conditions, with systematic addition of key ceramide structural features. Overall, a substantial increase in both sensitivity and fragmentation was observed on CID of $[M + Li]^+$ versus $[M + Na]^+$ of the same CMH components analyzed under similar conditions, and the method was found to be particularly effective for detailed structural analysis of fungal cerebrosides, especially minor structural variants present in mixtures at extremely low abundance.[31,32] Recently, Hsu and Turk[33] investigated the fragmentation of Li^+-adducted GSLs under these conditions in more detail, as well as applying in-source CID (i.e., product ion scans on primary fragments generated in the orifice region, essentially equivalent to ESI-$[CID\text{-}MS]^2$), parent ion scanning, and constant neutral loss scanning.

In preliminary studies[18,34,35] we have now applied Li^+ adduction to characterization of fungal GIPCs, and have observed a similar increase in sensitivity and fragmentation in product ion ESI-MS/CID-MS and ESI-$(CID\text{-}MS)^2$ mode. Precursor ion scanning from appropriate glycosylinositol phosphate product ions yielded clean molecular ion profiles in the presence of obscuring impurity peaks. Due to the different composition of the GIPC ceramides, which generally contain phytosphingosine (4-hydroxysphinganine) in

place of the (4*E*,8*E*)-sphing-4,8-dienine found as the major sphingoid of fungal cerebrosides, as well as the presence of the non-glycosidic and anionic inositol phosphate moiety interpolated between glycan and ceramide, a number of differences are observed in the fragmentation patterns of these compounds, characteristic for both the glycosylinositol and phytoceramide moieties with or without phosphate. In this paper, we describe applications of positive ion ESI-MS, -CID-MS, -MS/CID-MS, and -(CID-MS)^2 with Li^+ adduction to characterization of GIPC fractions of increasing structural complexity from a variety of fungi, including a non-pathogenic Basidiomycete (mushroom), *Agaricus blazei*, and pathogenic Euascomycete species such as *Aspergillus fumigatus, Histoplasma capsulatum*, and *Sporothrix schenckii*.

EXPERIMENTAL

Glycosylinositol phosphorylceramides

The cultures of *Sporothrix schenckii*, strain 65, and *Histoplasma capsulatum*, strain 496, were provided by Dr. Olga Gompertz, Department of Cellular Biology, Universidade Federal de São Paulo/Escola Paulista de Medicina, São Paulo, SP, Brasil. Conditions for growth of mycelium and yeast forms of these dimorphic species, and of mycelia of *Aspergillus fumigatus*, ATCC strain 9197, have been described previously.[32,36,37] Extraction and fractionation of neutral and acidic GSLs were carried out as described previously.[16,18,19] Preliminary characterizations of GIPC fractions **Ab-1**, a Manα1 → 2Ins-P-Cer (Mα2IPC; illustrated in Scheme 1) from the mushroom *Agaricus blazei*; **Ss-M1** (Manα1 → 6Ins-P-Cer; Mα6IPC), **Ss-M2** (Manα1 → 3Manα1 → 6Ins-P-Cer; Mα3Mα6IPC), **Ss-Y1/-Y2** (Manα1 → 3Manα1 → 2Ins-P-Cer; Mα3Mα2IPC), and **Ss-M3** (Manα1 → 3(Galβ1 → 4)Manα1 → 2Ins-P-Cer) from *S. schenckii* have been described (in all cases Ins-P = *myo*−inositol-1-phosphate, based on detailed NMR analysis and/or comparison of NMR spectra with those of compounds for which this component was unambiguously characterized by GC/MS methods).[16–19] Two GIPC fractions, designated **Hc-M3a** and **Hc-M3b**, corresponding to a component described by Barr *et al.*[13] as Manα1 → 3(Galβ1 → 4)Manα1 → 2 or → 6Ins-P-Cer, were isolated from the mycelium form of *H. capsulatum*, and confirmed to have the proposed glycosylinositol sequence with a Manα1 → 2Ins linkage, having both ^{1}H- and ^{13}C-NMR spectra essentially identical to those of fraction **Ss-M3** from *S. schenckii*.[18,19] Based on preliminary ^{1}H-NMR analysis, a GIPC fraction isolated from *A. fumigatus*, **Af-2**, is proposed to have the structure Manα1 → 3Manα1 → 2Ins-P-Cer (Mα3Mα2IPC); this is identical with respect to glycosylinositol sequence to **Ss-Y1/-Y2**, and to a compound previously isolated and fully characterized from *Paracoccidiodes brasiliensis*, **Pb-2**.[16] Designations and structures proposed for all GIPCs used in this study are summarized in Table 1.

Electrospray ionization mass spectrometry

ESI-MS and MS/MS experiments were performed in positive ion mode on a PE-Sciex (Concord, Ontario, Canada) API-III triple quadrupole mass spectrometer with a standard IonSpray source, using direct infusion (3 μL/min) of GIPC samples dissolved (~20 ng/μL) in 100% MeOH.[16,18,19,31,32] All single analyzer spectra were obtained by scanning Q1. Under these conditions, only sodiated molecular adducts were normally observed in ESI-MS in the absence of additives.[16,31,36,37] Appropriate amounts of Li^+ were determined empirically in ESI-MS profile mode (orifice-to-skimmer voltage (OR), 120–130 V; Ionspray voltage, 5 kV; interface temperature, 45 °C), by addition of a solution of LiI (10 mM) in MeOH until the observed ratio of $[M - H + 2Li]^+$ to $[M - H + Na + Li]^+$ was >95:5 (the final concentration of LiI was generally 4–5 mM). Single analyzer (high OR) ESI-CID-MS spectra were acquired with OR set ≥160 V. For product ion and precursor ion scanning ESI-MS/CID-MS, and for product ion scanning -(CID-MS)^2 experiments, OR was set to 100–130 and 160–180 V, respectively; the collision gas was argon (collision gas thickness [CGT] = 380–400 [$\times 10^{12}$ molecules/cm^2]), and collision energy was 80 eV.[31] Resolution parameters were set to achieve a peak width at 1/2 height of 0.6–0.7 Th (measured at *m/z* 332), deemed sufficient to assign nominal masses to all peaks in the mass range of interest. The appropriate mass range was scanned in *m/z* 0.1–0.25 steps, with a dwell time of 2.5 or 5 ms, depending on adjudged requirements of sample availability versus digital resolution and cycle time. In general, spectra represent summations of 5–10 scans for single analyzer profiles, and 10–30 scans for CID experiments (50–100 for some minor components), unless otherwise indicated.

Nomenclature

Ceramide fragment nomenclature is after Adams and Ann[23] (see Scheme 2(A)), except for some cases where additional

Table 1. Designations and structures for fungal glycosylinositol phosphorylceramide fractions analyzed or referred to in this study

Structure	Shorthand structure	Fraction	Source
Manα1 → 6Ins-P-Cer	Mα6IPC	**Ss-M1**	*S. schenckii*
Manα1 → 2Ins-P-Cer	Mα2IPC	**Ab-1**	*A. blazei*
Manα1 → 3Manα1 → 6Ins-P-Cer	Mα3Mα6IPC	**Ss-M2**	*S. schenckii*
Manα1 → 3Manα1 → 2Ins-P-Cer	Mα3Mα2IPC	**Af-2**	*A. fumigatus*
		Ss-Y1/-Y2	*S. schenckii*
		Pb-2	*P. brasiliensis*
Galβ1 → 4			
Manα1 → 2Ins-P-Cer	Mα3(Galβ4)Mα2IPC	**Ss-M3**	*S. schenckii*
Manα1 → 3		**Hc-M3**	*H. capsulatum*

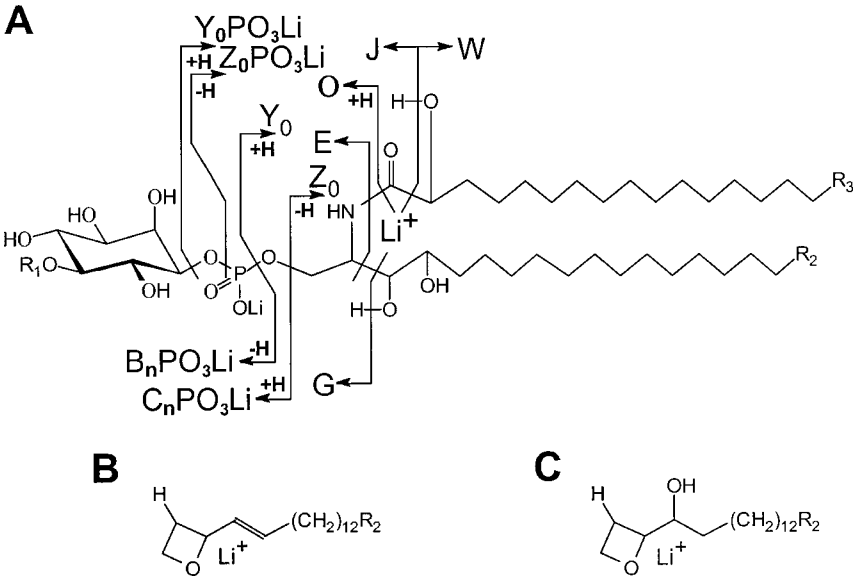

Scheme 2. Characteristic fragmentations of glycosylated IPCs. (A) Nomenclature of Adams and Ann[23] for fragmentation of ceramide moiety, and of Singh *et al.*[40] for *myo*-inositol phosphoryl group; (B) sphingoid $\underline{d}_{3b}$ ion, proposed by Hsu and Turk;[33] and (C) hydrated analog of $\underline{d}_{3b}$ ion, proposed in this study as a product of t18:0 phytosphingosine-containing ceramide.

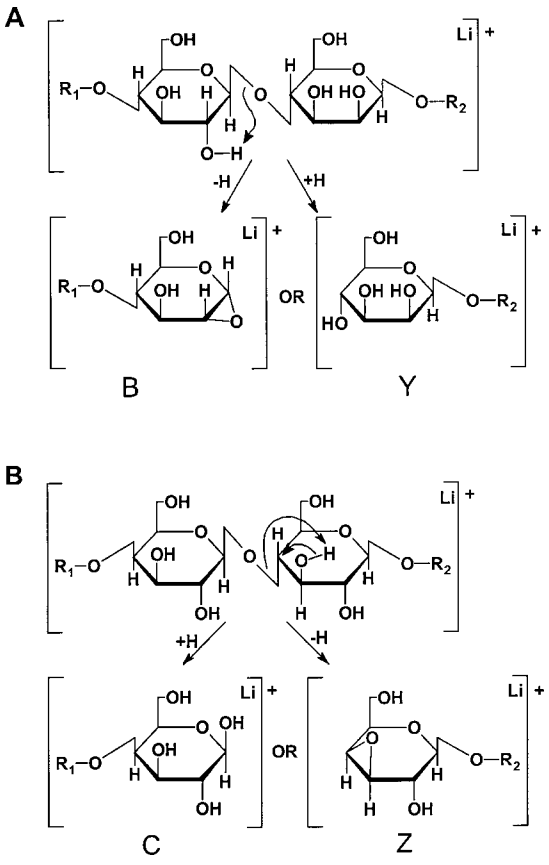

Scheme 3. Fragmentation of Li^+-adducted glycans with nomenclature according to Domon and Costello[45] and Costello and Vath.[22] (A) Production of B and Y fragments and (B) production of C and Z fragments. No definitive mechanism is implied. (Epoxide structures for B and Z ions are drawn according to Assam and Glish[46]).

fragments are given the designations used by Hsu and Turk[33] (Schemes 2(B),(C)). Glycan fragment nomenclature is after Costello *et al.*[22,38,39] (Scheme 3) as modified and expanded[40] for GIPCs (Schemes 2(A) and 4–6). In the following sections, the designation 'M' will be taken to refer to the monobasic salts of GIPCs, i.e., either $[M - H + Li]$ or $[M - H + Na]$; for fragment designations, the number of metal ions will be explicitly included, denoted by a parenthesis where exchanged, and by a plus sign where adducted, as adopted by Metelmann *et al.*[41] All *m/z* are designated with nominal, monoisotopic values. In all references to ESI experiments, the positive ion mode is implied except where otherwise indicated.

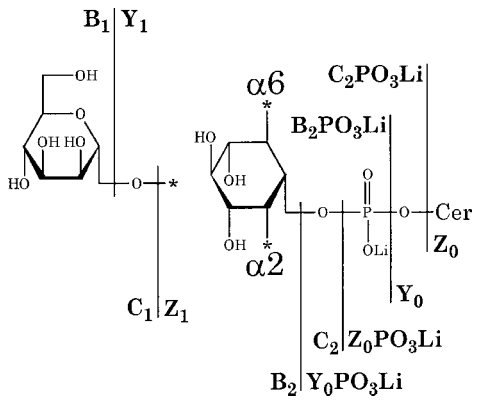

Scheme 4. Fragmentation of M(α2/α6)IPC, with nomenclature according to Costello and Vath,[22] as modified for GIPCs.[40] Hydrogen transfers as in Schemes 2 and 3 are omitted here.

RESULTS

Low OR ESI-MS, high OR ESI-CID-MS, and tandem ESI-MS/CID-MS experiments

Mannosylinositol phosphorylceramides. Ab-1 from Agaricus blazei

Because exchange of two metal ions (counterion and adducting ion) is required for conversion of any single GIPC molecular species to a homogeneous molecular adduct, there was some concern that addition of the required amount of LiI might result in concomitant suppression of the molecular ion signal before satisfactory adduction could be attained. In practice, however, it was possible to achieve >95% conversion of a disodiated GIPC to the dilithiated adduct with only slight suppression. Slightly higher orifice potentials (OR) seemed to be required for maximizing molecular ion signal with Li^+ compared to Na^+ adducts (120 V compared to 110 V). The result for **Ab-1**, the Mα2IPC from *A. blazei*, is illustrated in Fig. 1(A). Somewhat fortuitously, in this case, several ions not corresponding to molecular adducts of Mα2IPC were nearly ablated, but the total and relative signal amplitudes of the major molecular species ($[M + Li]^+$ at *m/z* 1072, 1100, and 1128 corresponding to $[M + Na]^+$ at *m/z* 1104, 1132, and 1160, respectively) were not significantly affected under otherwise identical acquisition conditions. The three molecular adducts differing by increments of *m/z* 28 correspond to ceramide variants differing by $2{\cdot}CH_2$ from each other in either sphingoid or fatty *N*-acyl components or both.

At higher orifice potentials, significant fragmentation could be induced, and OR = 180 V was routinely adopted for single quadrupole ESI-CID-MS scanning. In the single quadrupole high OR spectrum of lithiated **Ab-1** (Fig. 1(C)), an abundant trio of fragments at *m/z* 662, 690, and 718 were clearly observed in the spectrum, corresponding to $[Cer + Li]^+$ ($[Y_0 + Li]^+$) for the three molecular adducts; in addition, a pair of fragments at *m/z* 417 and 435 are consistent with the residue formula $[Hex{\cdot}Ins{\cdot}P{\cdot}Li_2]^+$ ($[B_2PO_3(Li) + Li]^+$ and $[C_2PO_3(Li) + Li]^+$, respectively; see Scheme 4). Interpretation of other fragments, few of which appear to be products of the Mα2IPC species in the sample, is less straightforward; as might be expected, this problem is effectively overcome by application of tandem ESI-MS/CID-MS experiments.

In applying low-energy tandem ESI-MS/CID-MS to characterization of GIPCs, we were particularly interested in determining whether there is any advantage to be gained from employing Li^+ adduction instead of analyzing the naturally occurring Na^+ adducts, a strategy which was previously used, for example, on GIPC components from *P. brasiliensis*.[16] Therefore ESI-MS/CID-MS product ion spectra with selection of molecular Li^+ adducts were compared directly with those acquired from the corresponding Na^+ adducts on the same day under essentially identical conditions (except for the small difference in OR, as noted above).

This is illustrated for one molecular species (**Ab-1c**) in Fig. 2, comparing the product ion spectrum of the Na^+ adduct *m/z* 1160 (A) with that of the corresponding Li^+ adduct *m/z* 1128 (B). In this case, lithiation appears to result in a slight decrease in overall signal intensity (as measured

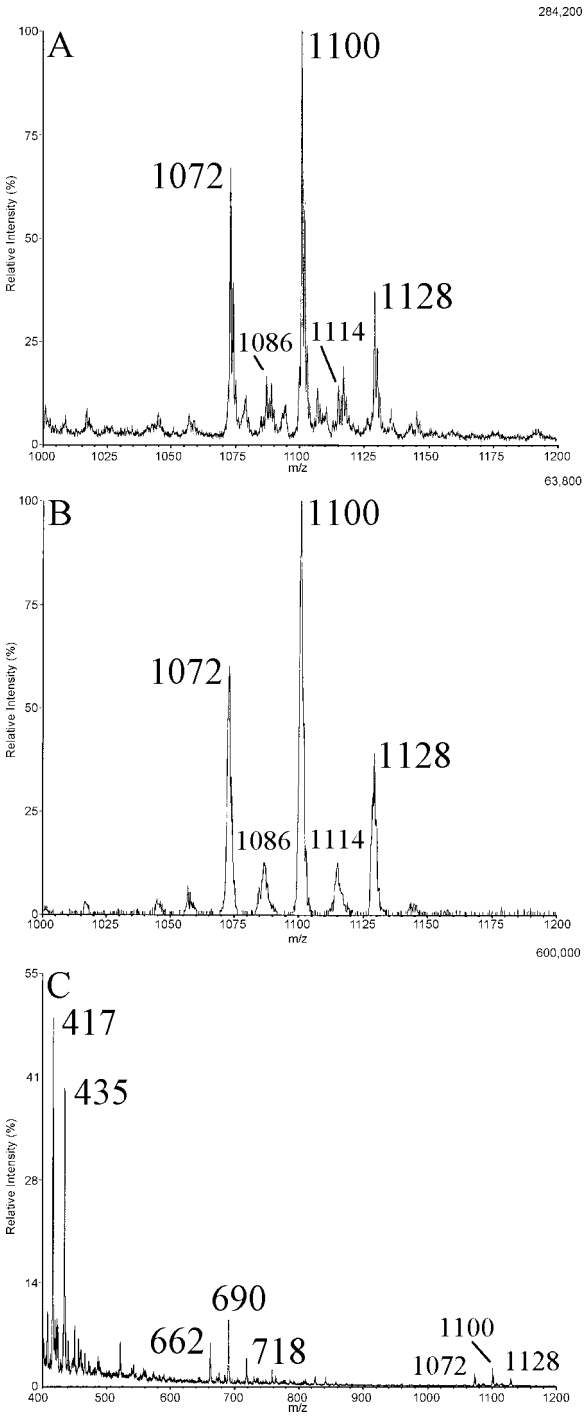

Figure 1. ESI-MS of MIPC from *Agaricus blazei* (**Ab-1**). (A) Low OR Li^+ adduct profile; (B) Li^+ adduct precursor ion profile, acquired in tandem ESI-MS/CID-MS mode with selection of *m/z* 435 in Q3; and (C) section of in-source ESI-CID-MS fragmentation spectrum acquired on Li^+ adducts at high OR.

by cpm of the base peak), but with an increase in both overall signal-to-noise and the abundance of several fragments, some of which are hardly observable in the Na^+ product ion spectrum. Among these are a number of product ions related to the ceramide moiety (summarized in Table 2(A)) at *m/z* 804, 786, 718, 700, and 420 ($[Y_0PO_3(Li) + Li]^+$, $[Z_0PO_3(Li) + Li]^+$, $[Y_0 + Li]^+$, $[Z_0 + Li]^+$,

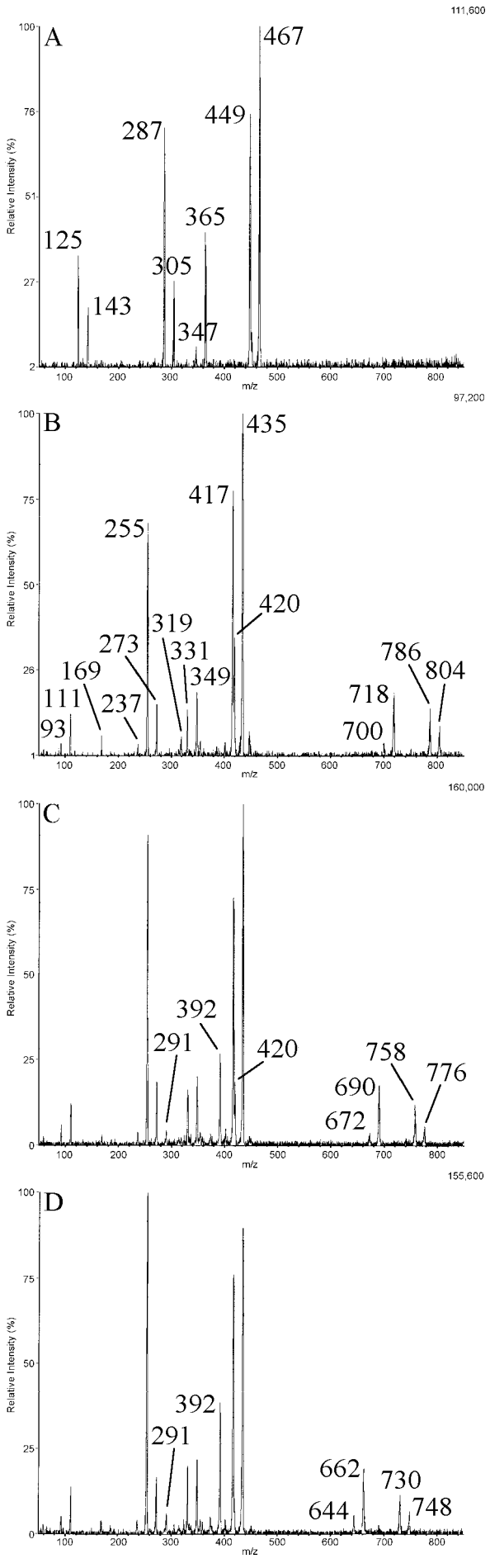

and $[O/Z_0PO_3(Li) + Li]^+$, respectively). Of the more prominent ceramide-related ions, the $[O/Z_0PO_3(Li) + Li]^+$ is particularly useful, since it provides key evidence for the mass of the sphingoid and, by subtraction from $[Z_0PO_3(Li) + Li]^+$, of the fatty *N*-acyl moiety as well. Here, the observation of these two ions at *m/z* 786 and 420, respectively, corresponds to a ceramide comprised of t20:0 sphingoid with h24:0 fatty *N*-acylation. Less abundant fragments appearing in the Li^+ adduct spectrum include *m/z* 402 ($[O/Z_0PO_3(Li) + Li - H_2O]^+$) and *m/z* 319, which is proposed to be a hydrated analog of the 'd_{3b}' fragment (see Schemes 2(B),(C)) observed by Hsu and Turk[33] at *m/z* 273 in ESI-MS/CID-MS and -(CID-MS)^2 product ion spectra of cerebrosides having d18:1 sphing-4-enine with 2-hydroxy fatty *N*-acylation. The putative d_{3b} fragment appears more prominently in ESI-(CID-MS)^2 spectra of $[Y_0 + Li]^+$ ions, and is observed at *m/z* 291 for GIPCs containing t18:0 phytosphingosine. Further discussion of these spectra is deferred until the last section.

Product ion spectra with selection of the other major Li^+ adducts at *m/z* 1100 (**Ab-1b**) and 1072 (**Ab-1a**) are reproduced in Figs 2(C) and 2(D), respectively. These show that the ceramide of the most abundant molecular species (*m/z* 1100; **Ab-1b**) contains both t18:0/h24:0 and t20:0/h22:0 components ($[Z_0PO_3(Li) + Li]^+$ at *m/z* 758; $[O/Z_0PO_3(Li) + Li]^+$ at *m/z* 392 and 420, respectively); while that of the lowest molecular mass species (*m/z* 1072; **Ab-1a**) is comprised primarily of a t18:0/h22:0 combination ($[Z_0PO_3(Li) + Li]^+$ at *m/z* 730; $[O/Z_0PO_3(Li) + Li]^+$ at *m/z* 392), with some t20:0/h20:0 also present ($[O/Z_0PO_3(Li) + Li]^+$ at *m/z* 420). These are essentially the expected results from random pairing of t18:0 and t20:0 sphingoids with h22:0 and h24:0 fatty acids. These data are not obtainable from NMR spectroscopy; they can be confirmed by GC/MS analysis, but with considerably more work and less detail.

With respect to fragmentation of the glycosylinositol of **Ab-1**, series of glycosidic cleavages with or without phosphate are well represented, and essentially identical in all three spectra (Figs 2(B)–(D); summarized in Table 3). An abundant pair of fragments is observed at *m/z* 417 and 435 for $[Hex \cdot Ins \cdot P \cdot Li_2]^+$ ($[B_2PO_3(Li) + Li]^+$ and $[C_2PO_3(Li) + Li]^+$, respectively); an additional pair representing $[Ins \cdot P \cdot Li_2]^+$ is observed at *m/z* 255 and 273 ($[Y_1/B_2PO_3(Li) + Li]^+$ and $[Y_1/C_2PO_3(Li) + Li]^+$, respectively). The bare phosphate moiety is represented by fragments *m/z* 93 and 111 ($[PO_3(Li) + Li]^+$ and $[H_2PO_4(Li) + Li]^+$), which appear to be the only fragments whose abundance is reduced by lithiation. Pairs of non-phosphorylated fragments representing the non-reducing end of the glycosylinositol are observed at *m/z* 169 and 187 for $[Hex + Li]^+$ ($[B_1 + Li]^+$ and $[C_1 + Li]^+$, respectively) and at *m/z* 331 and 349 for

Figure 2. Comparison of tandem ESI-MS/CID-MS product ion spectra from $[M + Na]^+$ or $[M + Li]^+$ of MIPC from *Agaricus blazei* (**Ab-1**). (A) Products of $[M + Na]^+$ at *m/z* 1160; (B) products of corresponding $[M + Li]^+$ at *m/z* 1128; (C) products of $[M + Li]^+$ at *m/z* 1100; and (D) products of $[M + Li]^+$ at *m/z* 1072 (unlabeled peaks in (B) and (C) have same *m/z* as corresponding peaks in (A)).

Table 2. Ceramide-related product ions (*m/z*) formed in low-energy ESI-MS/CID-MS (A) and ESI-(CID-MS)^2 (B) spectra of mannosyl-, dimannosyl-, and galactosyldimannosylinositol phosphorylceramides from the mushroom *A. blazei* (Ab), from mycelium and yeast forms of *S. schenckii* (Ss-M and Ss-Y, respectively), from the yeast form of *H. capsulatum* (Hc-M), and from mycelia of *A. fumigatus* (Af). Fragment designations as in Costello and Vath,[22] with modifications of Adams and Ann,[23] and Hsu and Turk,[33] illustrated in Schemes 2–5

Fraction:	**Ab-1a**	**Ab-1b1**	**Ab-1b2**	**Ab-1c**	**Ss-M1**	**Af-2a**	**Af-2b**	**Ss-M2**	**Ss-Y1a**	**Ss-Y1b**	**Ss-Y2a**	**Ss-Y2b**[e]	**Hc-M3a**	**Hc-M3b**	**Ss-M3**
Fatty acid:	h22:0	h24:0	h22:0	h24:0	h24:0	24:0	24:0	h24:0	h24:0	h24:0	2h24:0	2h24:0	h24:0	2h24:0	h24:0
Sphingoid:	t18:0	t18:0	t20:0	t20:0	t18:0	t18:0	t20:0	t18:0	t18:0	t20:0	t18:0	t20:0	t18:0	t18:0	t18:0
A. Products of $[M + Li]^+$:	1072	1100	1100	1128	1100	1246	1274	1262	1262	1290	1278	1306	1424	1440	1424
$[Y_0PO_3(Li) + Li]^+$	748	776	776	804	776	760	788	776	776	804	792	820	776	792	776
$[Z_0PO_3(Li) + Li]^+$	730	758	758	786	758	742	770	758	758	786	774	802	758V[d]	774	758V[d]
$[Z_0PO_3(Li) + Li - H_2O]^+$	712W[a]	740W	740W	ND[b]	740W	724	752	740W	ND	768W	ND	ND	740V	ND	740V
$[Y_0 + Li]^+$	662	690	690	718	690	674	702	690	690	718	706	734	690	706	690
$[Z_0 + Li]^+$	644	672	672	700	672	656	684	672	672	700	688	716	672V	688	672V
$[Z_0+Li - H_2O]^+$	ND	ND	ND	ND	ND	638	666	ND	ND	682W	ND	ND	656V	ND	656V
$[O/Z_0PO_3(Li) + Li]^+$	392	392	420	420	392	ND	ND	392	392	420	392	420[e]	392	392	392
B. Products of $[Y_0 + Li]^+$:	662	690	690	718	690	674	702	690	690	718	706	734	690	706	690
$[J/Y_0+Li - H_2O]^+$	334	334	362	362	334	----[c]	----	334	334	362	334	362	334	334	334
$[N + Li]^+$	324	324	352	352	324	----	----	324	324	352	324	352[e]	324	324	324
$[N + Li - H_2O]^+$	306	306	334	334	306	----	----	306	306	334	306	334	306	306	306
$[N + Li - 2H_2O]^+$	288	288	316	316	288	----	----	288	288	316	288	316	288	288	288
$\underline{d}_{3b}$	291	291	319	319	291	----	----	291	291	319	291	319	291	291	291
$[N + Li - H_2O - CH_2O]^+$	276	276	304	304	276	----	----	276	276	304	276	304	276	276	276
$\underline{d}_{3b} - H_2O$	263	263	291	291	263	----	----	263	263	263	263	263	263	263	263

[a] W = weak;
[b] ND = not detected;
[c] — = not determined;
[d] V = overlapped with major glycosylinositol ions;
[e] in addition to the major species (**Ss-Y2b1**), this component contains a small amount of a second species (**Ss-Y2b2**), with 2h26:0/t18:0 ceramide, as evidenced by low abundance ions for $[O/Z_0PO_3(Li) + Li]^+$ at *m/z* 392 in ESI-MS/CID-MS, and for $[N + Li]^+$ at *m/z* 324 in ESI-(CID-MS)^2.

RCM

$[Hex \cdot Ins + Li]^+$ ($[B_2 + Li]^+$ and $[C_2 + Li]^+$). The lineage of these fragments could be confirmed by acquisition of ESI-$(CID\text{-}MS)^2$ product ion spectra with selection of the phosphorylglycosylinositol primary fragments at *m/z* 417 and 435 (see later section).

Precursor ion scanning in ESI-MS/CID-MS mode, with selection in Q3 of phosphorylglycosylinositol primary fragments at *m/z* 417 and 435, effectively yielded $[M + Li]^+$ profiles free of contributions from interfering impurities (Fig. 1(B)). These profiles clearly exhibited less abundant molecular species differing by ±14 Th from those already noted, corresponding to minor components having odd carbon-numbered sphingoid or fatty *N*-acyl groups. Interestingly, a second cluster of precursor ions, in which the masses of all species differed from those in the main group by +134 Th, was also observed (not shown); the major species was found at *m/z* 1234, appearing at ~3–5% of the abundance at *m/z* 1100. It is most likely that these ions result from attachment of LiI (M = 133.85).

Ss-M1 from Sporothrix schenckii

The availability of **Ss-M1**, the Mα6IPC from the mycelium form of *S. schenckii*, afforded an opportunity to compare results from a naturally occurring isomer of **Ab-1**. The sample of **Ss-M1** was more limited in amount and purity, as can be seen from a profile of the expected molecular ion region, prior to lithiation, reproduced in Fig. 3(A). In this profile, no Na^+ adducts with reasonable values of *m/z* for a MIPC are visible above interfering impurity peaks. Following addition of LiI, a major $[M + Li]^+$ species clearly emerges at *m/z* 1100 (Fig. 3(B)). The situation was further clarified by precursor ion scanning in ESI-MS/CID-MS mode, with selection in Q3 of the expected primary fragment *m/z* 417 (see below), which yielded the $[M + Li]^+$ profile shown in Fig. 3(C)). This profile clearly showed only a single abundant molecular species *m/z* 1100, consistent with a MIPC having either a t18:0/h24:0 or t20:0/h22:0 ceramide component, or both, as determined for **Ab-1b** above. Additional components differing from this by ±n·14 Th (n = 1 or 2) correspond to minor ceramide variants having other carbon-numbered sphingoid or fatty *N*-acyl groups; furthermore, components differing from the major one by ±16 Th suggest the presence of minor ceramide variants with different levels of hydroxylation. A likely LiI attachment ion can be observed (*m/z* 1234) in both the single analyzer profile (Fig. 3(B)) and the precursor ion spectrum (Fig. 3(C)).

The single quadrupole high OR spectrum of lithiated **Ss-M1** (Fig. 4(A)) immediately produced an interesting result as, aside from the expected $[Y_0 + Li]^+$ fragment at *m/z* 690, it is dominated by the $[B_2PO_3(Li) + Li]^+$ fragment *m/z* 417. Compared with the single analyzer spectrum of the isomeric Mα2IPC **Ab-1** (Fig. 1(C)), the $[C_2PO_3(Li) + Li]^+$ fragment at *m/z* 435 is of extremely low abundance here. This difference is accentuated in the tandem ESI-MS/CID-MS spectrum of the products of *m/z* 1100 (Fig. 4(B); compare spectra in Figs 2(B), 2(C) and 2(D)). All other ions observed in the CID spectra of **Ab-1** $[M + Li]^+$ are present in the spectrum of **Ss-M1**, but at much lower relative abundance. The striking difference in abundance ratios of *m/z* 417 versus 435 indicates a highly significant difference in activation of the fragmentation reactions leading to these ions in the two isomeric structures.

With respect to the ceramide moiety of **Ss-M1**, the $[Z_0PO_3(Li) + Li]^+$ at *m/z* 758, accompanied by the $[O/Z_0PO_3(Li) + Li]^+$ at *m/z* 392 (with *m/z* 420 apparently absent), implies a fairly homogeneous t18:0/h24:0 composition for the major *m/z* 1100 component. This could be confirmed by ESI-$(CID\text{-}MS)^2$ with selection of the major ceramide $[Y_0 + Li]^+$ fragment at *m/z* 690 (see later section).

Dimannosylinositol phosphorylceramides. Af-2 from Aspergillus fumigatus

The low OR single analyzer profile of lithiated **Af-2**, a Mα3Mα2IPC from *A. fumigatus*, is reproduced in Fig. 5(A). The profile consists of two major $[M + Li]^+$ at *m/z* 1246 and 1274 in ~2:1 abundance ratio; these $[M + Li]^+$ are consistent with a composition of $Hex_2 \cdot Ins \cdot P$ linked to ceramides differing by $2 \cdot CH_2$ from each other in either sphingoid or fatty acid components; both *m/z* also differ from the expected values for even C-numbered 2-hydroxy fatty-*N*-acyl-4-hydroxysphinganines by a decrement of 16 Th, corresponding to one hydroxyl group missing from either the fatty *N*-acyl or sphingoid component. At high OR, fragments at *m/z* 417, 435, 579, 597, 674, and 702 were observed in the spectrum (not shown), corresponding to $[Hex \cdot Ins \cdot P \cdot Li_2]^+$ ($[Y_2/B_3PO_3(Li) + Li]^+$ and $[Y_2/C_3PO_3(Li) + Li]^+$), $[Hex_2 \cdot Ins \cdot P \cdot Li_2]^+$ ($[B_3PO_3(Li) + Li]^+$ and $[C_3PO_3(Li) + Li]^+$), and a pair of $[Cer + Li]^+$ ($[Y_0 + Li]^+$), respectively (see Scheme 5, Table 3). The presence of numerous impurity peaks made it difficult to identify any further ions. On the other hand, tandem ESI-MS/CID-MS of both the *m/z* 1274 (Fig. 5(C)) and 1246 components yielded strong product spectra, virtually identical except for those ions related to the ceramide or phosphorylceramide moieties, which differed by a uniform increment of *m/z* 28 between the two components. In addition to the phosphorylglycosylinositol fragments already mentioned, pairs of fragments from glycosidic cleavages are also observed at *m/z* 169 and 187 ($[B_1 + Li]^+$ and $[C_1 + Li]^+$), *m/z* 331 and 349 ($[B_2 + Li]^+$ or $[Y_2/B_3 + Li]^+$ and $[C_2 + Li]^+$ or $[Y_2/C_3 + Li]^+$), *m/z* 255 and 273 ($[Y_1/B_3PO_3(Li) + Li]^+$ and $[Y_1/C_3PO_3(Li) + Li]^+$), and *m/z* 493 and 511 ($[B_3 + Li]^+$ and $[C_3 + Li]^+$), along with the minor dehydration product at *m/z* 237 $[Y_1/B_3PO_3(Li) + Li - H_2O]^+$. Particularly worth noting are the abundance ratios of the *m/z* 417/435 and 579/597 pairs, which are ~0.8:1 and ~0.4:1, respectively, with *m/z* 597 being overall the base peak (see below).

With respect to ceramide fragments, interestingly, no $[O/Z_0PO_3(Li) + Li]^+$ ion could be observed in either spectrum. A precursor ion CID spectrum with selection of *m/z* 597 in Q3 yielded a clean $[M + Li]^+$ profile (Fig. 5(B)), which showed a clear contribution to *m/z* 1290 from a component with an additional oxygen atom. Product ion scanning with selection of this $[M + Li]^+$ (not shown) gave a weak but definite mass spectrum similar to those discussed, but exhibiting as well a peak at *m/z* 420 ($[O/Z_0PO_3(Li) + Li]^+$ ion corresponding to a t20:0/h24:0 ceramide component). Subsequent component analysis by GC/MS, besides confirming that **Af-2** contains mannose as the sole sugar constituent, showed that by far the major fatty acid

Table 3. Glycosylinositol- and phosphorylglycosylinositol-related product ions formed in low-energy ESI-MS/CID-MS and ESI-(CID-MS)^2 spectra of mannosyl-, dimannosyl-, and galactosyldimannosylinositol phosphorylceramides from the mushroom *A. blazei* (Ab), from mycelium and yeast forms of *S. schenckii* (Ss-M and Ss-Y, respectively), from the yeast form of *H. capsulatum* (Hc-M), and from mycelia of *A. fumigatus* (Af). Base peak distinguished by bold font. Fragment designations as in Costello and Vath,[22] as expanded for GIPCs in Singh *et al.*[40] illustrated in Schemes 3–5

m/z	Ab-1a,b,c	Ss-M1	Ss-M2 Ss-Y1b, Ss-Y2a,b	Af-2a,b Ss-Y1a, Ss-Y2a,b	Ss-M3 Hc-M3a,b
759					**$[C_3PO_3(Li) + Li]^+$**
741					$[B_3PO_3(Li) + Li]^+$
673					$[C_3 + Li]^+$
655					$[B_3 + Li]^+$
597			$[C_3PO_3(Li) + Li]^+$	**$[C_3PO_3(Li) + Li]^+$**	$[Y_{2\alpha \text{ or } \beta}/C_3PO_3(Li) + Li]^+$
579			**$[B_3PO_3(Li) + Li]^+$**	$[B_3PO_3(Li) + Li]^+$	$[Y_{2\alpha \text{ or } \beta}/B_3PO_3(Li) + Li]^+$
561			$[B_3PO_3(Li) + Li - H_2O]^+$	$[B_3PO_3(Li) + Li - H_2O]^+$	$[Y_{2\alpha \text{ or } \beta}/B_3PO_3(Li) + Li - H_2O]^+$
511			$[C_3 + Li]^+$	$[C_3 + Li]^+$	$[Y_{2\alpha \text{ or } \beta}/C_3 + Li]^+$ or $[C_2 + Li]^+$
493			$[B_3 + Li]^+$	$[B_3 + Li]^+$	$[Y_{2\alpha \text{ or } \beta}/B_3 + Li]^+$ or $[B_2 + Li]^+$
477			$[^{0,2}X_3/C_3PO_3(Li) + Li]^+$		
459			$[^{0,2}X_3/B_3PO_3(Li) + Li]^+$		
435	**$[C_2PO_3(Li) + Li]^+$**	$[C_2PO_3(Li) + Li]^+$	$[Y_2/C_3PO_3(Li) + Li]^+$	$[Y_2/C_3PO_3(Li) + Li]^+$	$[Y_{2\alpha}/Y_{2\beta}/C_3PO_3(Li) + Li]^+$
417	$[B_2PO_3(Li) + Li]^+$	**$[B_2PO_3(Li) + Li]^+$**	$[Y_2/B_3PO_3(Li) + Li]^+$	$[Y_2/B_3PO_3(Li) + Li]^+$	$[Y_{2\alpha}/Y_{2\beta}/B_3PO_3(Li) + Li]^+$
399	$[B_2PO_3(Li) + Li - H_2O]^+$	$[B_2PO_3(Li) + Li - H_2O]^+$	$[Y_2/B_3PO_3(Li) + Li - H_2O]^+$	$[Y_2/B_3PO_3(Li) + Li - H_2O]^+$	$[Y_{2\alpha}/Y_{2\beta}/B_3PO_3(Li) + Li - H_2O]^+$
349	$[C_2 + Li]^+$	$[C_2 + Li]^+$	$[Y_2/C_3 + Li]^+$ or $[C_2 + Li]^+$	$[Y_2/C_3 + Li]^+$ or $[C_2 + Li]^+$	$[Y_{2\alpha}/Y_{2\beta}/C_3 + Li]^+$ or $[Y_{2\alpha \text{ or } \beta}/C_2 + Li]^+$
331	$[B_2 + Li]^+$	$[B_2 + Li]^+$	$[Y_2/B_3 + Li]^+$ or $[B_2 + Li]^+$	$[Y_2/B_3 + Li]^+$ or $[B_2 + Li]^+$	$[Y_{2\alpha}/Y_{2\beta}/B_3 + Li]^+$ or $[Y_{2\alpha \text{ or } \beta}/B_2 + Li]^+$
273	$[Y_1/C_2PO_3(Li) + Li]^+$	$[Y_1/C_2PO_3(Li) + Li]^+$	$[Y_1/C_3PO_3(Li) + Li]^+$	$[Y_1/C_3PO_3(Li) + Li]^+$	$[Y_1/C_3PO_3(Li) + Li]^+$
255	$[Y_1/B_2PO_3(Li) + Li]^+$	$[Y_1/B_2PO_3(Li) + Li]^+$	$[Y_1/B_3PO_3(Li) + Li]^+$	$[Y_1/B_3PO_3(Li) + Li]^+$	$[Y_1/B_3PO_3(Li) + Li]^+$
237	$[Y_1/B_2PO_3(Li) + Li - H_2O]^+$	$[Y_1/B_2PO_3(Li) + Li - H_2O]^+$	$[Y_1/B_3PO_3(Li) + Li - H_2O]^+$	$[Y_1/B_3PO_3(Li) + Li - H_2O]^+$	$[Y_1/B_3PO_3(Li) + Li - H_2O]^+$
187	$[Y_1/C_2 + Li]^+$ or $[C_1 + Li]^+$	$[Y_1/C_2 + Li]^+$ or $[C_1 + Li]^+$	$[Y_1/C_3 + Li]^+$ or $[C_1 + Li]^+$	$[Y_1/C_3 + Li]^+$ or $[C_1 + Li]^+$	$[Y_1/C_3 + Li]^+$ or $[C_{1\alpha \text{ or } \beta} + Li]^+$
169	$[Y_1/B_2 + Li]^+$ or $[B_1 + Li]^+$	$[Y_1/B_2 + Li]^+$ or $[B_1 + Li]^+$	$[Y_1/B_3 + Li]^+$ or $[B_1 + Li]^+$	$[Y_1/B_3 + Li]^+$ or $[B_1 + Li]^+$	$[Y_1/B_3 + Li]^+$ or $[B_{1\alpha \text{ or } \beta} + Li]^+$
111	$[LiH_2PO_4 + Li]^+$	$[LiH_2PO_4 + Li]^+$	$[LiH_2PO_4 + Li]^+$	$[LiH_2PO_4 + Li]^+$	$[LiH_2PO_4 + Li]^+$
93	$[LiPO_3 + Li]^+$	$[LiPO_3 + Li]^+$	$[LiPO_3 + Li]^+$	$[LiPO_3 + Li]^+$	$[LiPO_3 + Li]^+$

RCM

constituent was tetradocosanoate (24:0), with only a small amount of 2-hydroxytetradocosanoate (h24:0) present. Two phytosphingosines were detected in this analysis, t18:0 and t20:0, clearly demonstrating that the two major $[M + Li]^+$ ions in the profile of **Af-2** correspond to t18:0/24:0 and t20:0/24:0 ceramide species, and that the failure to detect significant $[O/Z_0PO_3(Li) + Li]^+$ ions in the CID spectra of these components is due to the absence of 2-hydroxylation of the fatty acid, rather than any missing from the sphingoid moiety.

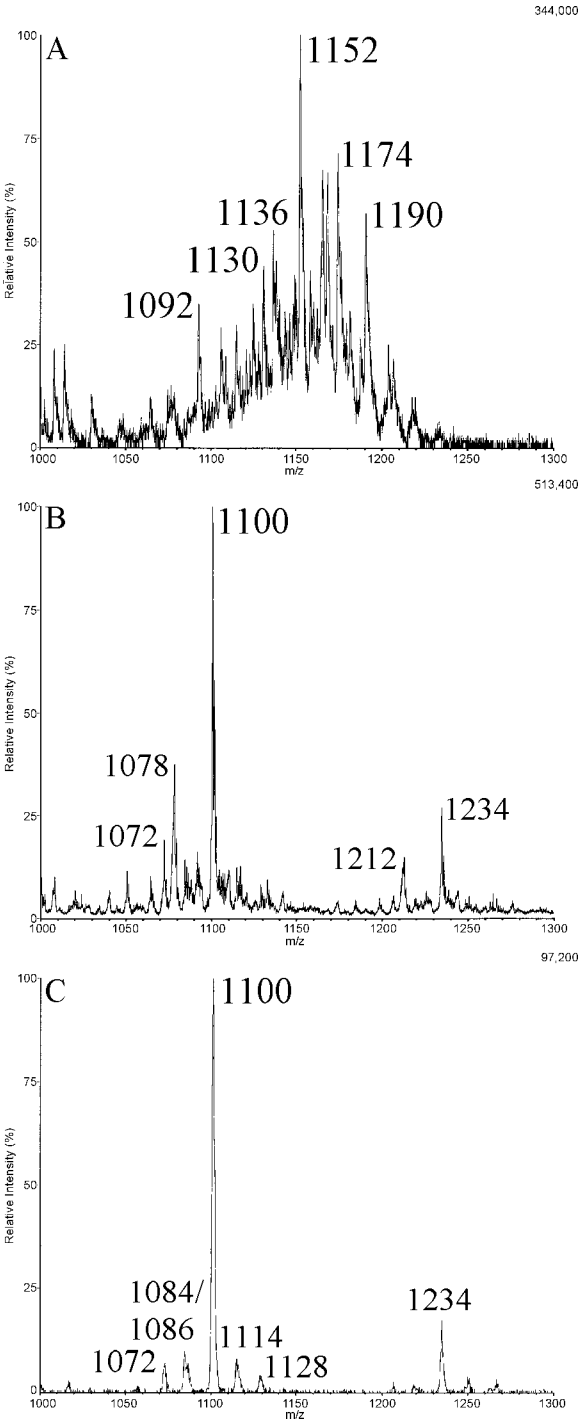

Figure 3. ESI-MS of MIPC from mycelium form of *Sporothrix schenckii* (**Ss-M1**). (A) Low OR Na^+ adduct profile; (B) low OR Li^+ adduct profile; and (C) Li^+ adduct precursor ion profile, acquired in tandem ESI-MS/CID-MS mode with selection of *m/z* 417 in Q3.

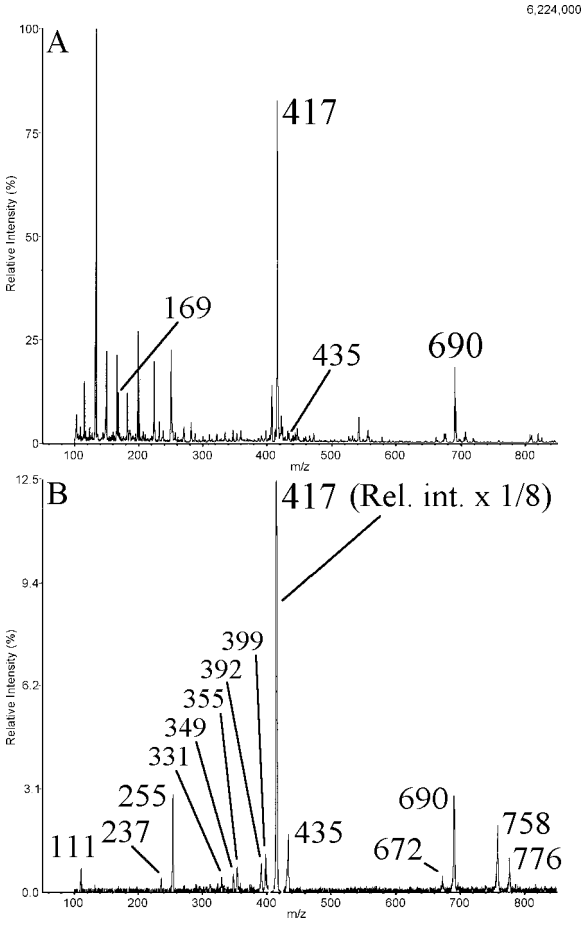

Figure 4. Comparison of single analyzer and tandem mass spectra of MIPC from mycelium form of *Sporothrix schenckii* (**Ss-M1**). (A) In-source ESI-CID-MS fragmentation spectrum acquired on Li^+ adducts at high OR and (B) tandem ESI-MS/CID-MS product ion spectrum from $[M + Li]^+$ at *m/z* 1100 (note that abundance of peak at *m/z* 417 only has been attenuated by a factor of 8 compared with the rest of the spectrum).

Ss-M2 from Sporothrix schenckii

The low OR single analyzer profile of lithiated **Ss-M2**, a Mα3Mα6IPC from the mycelium form of *S. schenckii*, is reproduced in Fig. 6(A). The profile consisting of a single major $[M + Li]^+$ ion at *m/z* 1262 is similar to that of **Ss-M1**, but with an increment of +162 Th corresponding to the additional Hex unit. At high OR, fragments at *m/z* 417, 579 and 690 were observed in the spectrum (not shown), corresponding to $[Hex \cdot Ins \cdot P \cdot Li_2]^+$ ($[Y_2/B_3PO_3(Li) + Li]^+$), $[Hex_2 \cdot Ins \cdot P \cdot Li_2]^+$ ($[B_3PO_3(Li) + Li]^+$), and $[Cer + Li]^+$ ($[Y_0 + Li]^+$), respectively, but the presence of numerous impurity peaks obscured the lower *m/z* regions. Notable, however, was the virtual absence of $[Y_2/C_3PO_3(Li) + Li]^+$ and $[C_3PO_3(Li) + Li]^+$ ions at *m/z* 435 and 597. In agreement with this, the major product ion from ESI-MS/CID-MS of *m/z* 1262 (Fig. 6(C)) is that at *m/z* 579 (base peak); compared with this, no other fragment is present in greater than 15% abundance. In contrast to the product ion spectra from

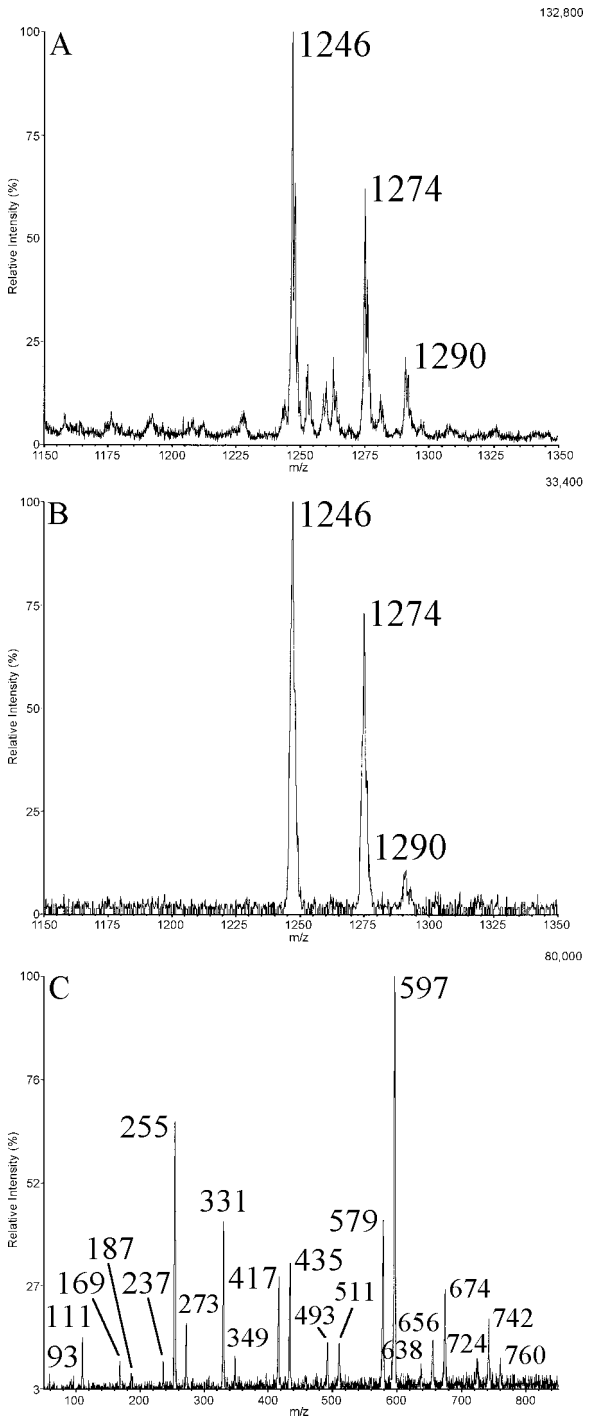

Figure 5. ESI-MS of M_2IPC from *Aspergillus fumigatus* (**Af-2**). (A) Low OR Li^+ adduct profile; (B) Li^+ adduct precursor ion profile, acquired in tandem ESI-MS/CID-MS mode with selection of *m/z* 597 in Q3; and (C) tandem ESI-MS/CID-MS product ion spectra from $[M + Li]^+$ at *m/z* 1274.

$[M + Li]^+$ of **Af-2**, the abundance ratio of the *m/z* 579/597 pair is 17:1, while the $[Y_2/C_3PO_3(Li) + Li]^+$ ion at *m/z* 435 is virtually absent. Another notable difference is the appearance of an ion at *m/z* 459, consistent with a fragment including an internal sugar ring cleavage, $[^{0,2}X_3/B_3PO_3(Li) + Li]^+$ (see Scheme 5). A much less abundant ion at *m/z* 477 may correspond to $[^{0,2}X_3/C_3PO_3(Li) + Li]^+$. The remainder of the spectrum is similar to those from $[M + Li]^+$ of **Af-2** (Table 3).

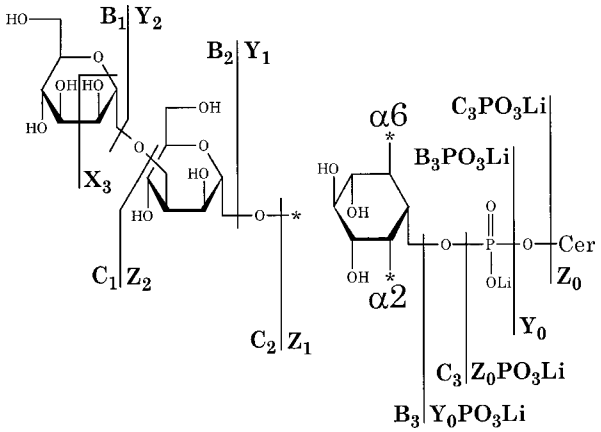

Scheme 5. Fragmentation of Mα3M(α2/α6)IPC, with nomenclature according to Costello and Vath,[22] as modified for GIPCs.[40] Hydrogen transfers as in Schemes 2 and 3 are omitted here.

The trend in $[B_3PO_3(Li) + Li]^+/[C_3PO_3(Li) + Li]^+$ abundance ratios when comparing the product ion spectra of **Ss-M2** and **Af-2** is analogous to that already noted above for the $[B_2PO_3(Li) + Li]^+/[C_2PO_3(Li) + Li]^+$ ratios comparing spectra for **Ss-M1** and **Ab-1**, reinforcing the conclusion that the abundance of these ions is strongly influenced by the linkage of the first Man to the Ins residue, Mα6Ins versus Mα2Ins. It will be interesting to see whether GIPCs with other linkages of Man to Ins, if they exist, exhibit other interpretable differences in their fragmentation spectra.

With respect to fragments derived from ceramide, these and their interpretations are similar to those observed for **Ss-M1** (Table 2(A)). Scanning for precursors of the ions *m/z* 579 (Fig. 6(B)), 417, and 255 again showed that the only major molecular species in fraction **Ss-M2** giving rise to these products is the one observed at *m/z* 1262. A likely LiI attachment ion can be observed at *m/z* 1396.

Ss-Y1 and Ss-Y2 from Sporothrix schenckii

Two dimannosylinositol phosphorylceramide fractions isolated from the yeast form of *S. schenckii*, that have distinct Rf values in HPTLC, presented a more difficult analytical problem. They were available in limited amounts, and, although 1-D ^{1}H-NMR spectroscopy indicated the major component in each fraction with respect to glycosylinositol structure was Mα3Mα2Ins, numerous impurities were also detected, including resonances consistent with minor amounts of Mα3Mα6IPC. In contrast to **Ss-M2**, the Mα3-Mα6IPC fraction isolated from the mycelium form, **Ss-Y1** and **Ss-Y2** presented two major $[M + Li]^+$ each, at *m/z* 1262 and 1290 for the former, and at *m/z* 1278 and 1306 for the latter (Figs 7(A) and 7(C)). Within each fraction, the two major $[M + Li]^+$ differ from each other by a 28 Th increment, representing 2·CH_2 in either the sphingoid or fatty *N*-acyl component. Furthermore, the major $[M + Li]^+$ ions in **Ss-Y2** differ from those in **Ss-Y1** by a 16 Th increment, representing an additional hydroxyl group on either the sphingoid or fatty-*N*-acyl moiety. A ESI-MS/CID-MS product ion spectrum of the major **Ss-Y1** *m/z* 1290 component (Fig. 8(A)) exhibits a set of glycosylinositol and glycosylphosphoryl-

inositol fragments very similar in *m/z* and abundance to those of the Mα3Mα2IPC **Af-2**. The ceramide-related fragments are those observed for **Ab-1c**, including the $[Z_0PO_3(Li) + Li]^+$ and $[O/Z_0PO_3(Li) + Li]^+$ ions at *m/z* 786 and 420, respectively, corresponding to t20:0/h24:0 ceramide. The product ion spectrum for the minor *m/z* 1262 component (Fig. 8(B)) was weak, but the $[Z_0PO_3(Li) + Li]^+$ and $[O/Z_0PO_3(Li) + Li]^+$ ions at *m/z* 758 and 392, respectively, clearly indicate the presence of t18:0/h24:0 ceramide. Interestingly, the pattern of glycosylinositol and glycosylphosphorylinositol fragments (low abundance of *m/z* 597 and 435, presence of *m/z* 459) suggests that it contains mostly Mα3Mα6IPC. A similar analysis of the two major **Ss-Y2** $[M + Li]^+$ ions at *m/z* 1306 and 1278 (Figs 8(C) and 8(D)) shows that both are mixtures of Mα3Mα2IPC and Mα3-Mα6IPC, but with the higher molecular mass component containing more of the former (*m/z* 597 more abundant than *m/z* 579). The differences in the latter fraction are not quite as pronounced as those observed for **Ss-Y1**. These results explain why precursor ion scans from *m/z* 579 (Figs 7(B) and 7(D)) display molecular adduct profiles quantitatively different from those obtained via single analyzer for both of these fractions (Figs 7(A) and 7(C)), and highlight the need for caution in quantitative interpretation of molecular profiles generated from precursor ion scanning.

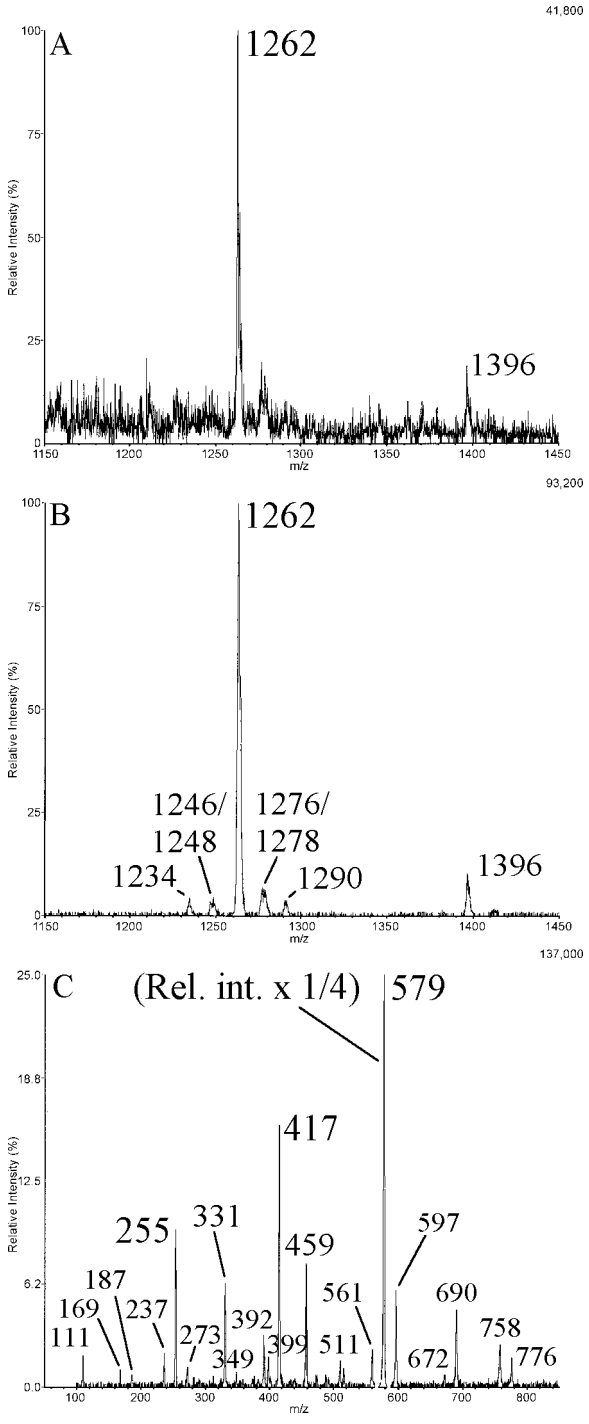

Figure 6. ESI-MS of M_2IPC from mycelium form of *Sporothrix schenckii* (**Ss-M2**). (A) Low OR Li^+ adduct profile; (B) Li^+ adduct precursor ion profile, acquired in tandem ESI-MS/CID-MS mode with selection of of *m/z* 579 in Q3; and (C) tandem ESI-MS/CID-MS product ion spectrum from $[M + Li]^+$ at *m/z* 1262 (note that abundance of peak at *m/z* 579 only has been attenuated by a factor of 4 compared with the rest of the spectrum).

Notable also, in the case of fraction **Ss-Y2**, are the predominant $[O/Z_0PO_3(Li) + Li]^+$ ions at *m/z* 420 and 392 for its two components, respectively; these indicate that the additional hydroxylation must in both cases be carried by the fatty-*N*-acyl moieties (ceramide-related data for **Ss-Y1** and **Ss-Y2** components are summarized in Table 2(A)). Conclusions regarding the ceramide structures were confirmed by acquisition of ESI-(CID-MS)^2 product ion spectra with selection of primary $[Y_0 + Li]^+$ ions (see later section).

Triglycosylinositol phosphorylceramides. Hc-M3 from Histoplasma capsulatum *and Ss-M3 from* Sporothrix schenckii

A third fraction from the mycelium form of *S. schenckii*, **Ss-M3**, has been assigned the structure Manα1 → 3(Galβ1 → 4)Manα1 → 2Ins-P-Cer based on preliminary analysis of NMR data.[19] These data were essentially identical, with respect to glycan resonances, to those acquired (Toledo, Levery, Straus and Takahashi, unpublished results) for a triglycosyl InsPCer component previously found in both yeast and mycelium forms of *Histoplasma capsulatum*,[12] which was assigned the structure Manα1 → 3(Galβ1 → 4)Manα1 → 2 or 6Ins-P-Cer by Barr *et al.*[13] Since the point of ambiguity in the *H. capsulatum* GIPC structure had been the Man → Ins linkage position, it was of some interest to see if the 1 → 2, rather than 1 → 6, linkage could be confirmed in these compounds by mass spectrometric analysis. Two fractions of the triglycosyl InsPCer isolated from the mycelium form of *H. capsulatum*, **Hc-M3a** and **Hc-M3b**, with distinct Rf values in HPTLC, were therefore analyzed by ESI-MS after Li^+ adduction.

The low OR single analyzer profiles of **Hc-M3a** and **Hc-M3b** (see Fig. 9) were each observed as single major $[M + Li]^+$, at *m/z* 1424 and 1440, respectively. The molecular mass profile of **Hc-M3a** (Fig. 9(B)) was therefore similar to **Ss-M2**, but with an increment of +162 Th corresponding to the additional Hex unit; the molecular mass of **Hc-M3b** (Fig. 9(A)) then differed by a further increment of +16 Th, representing an additional hydroxyl group on either the

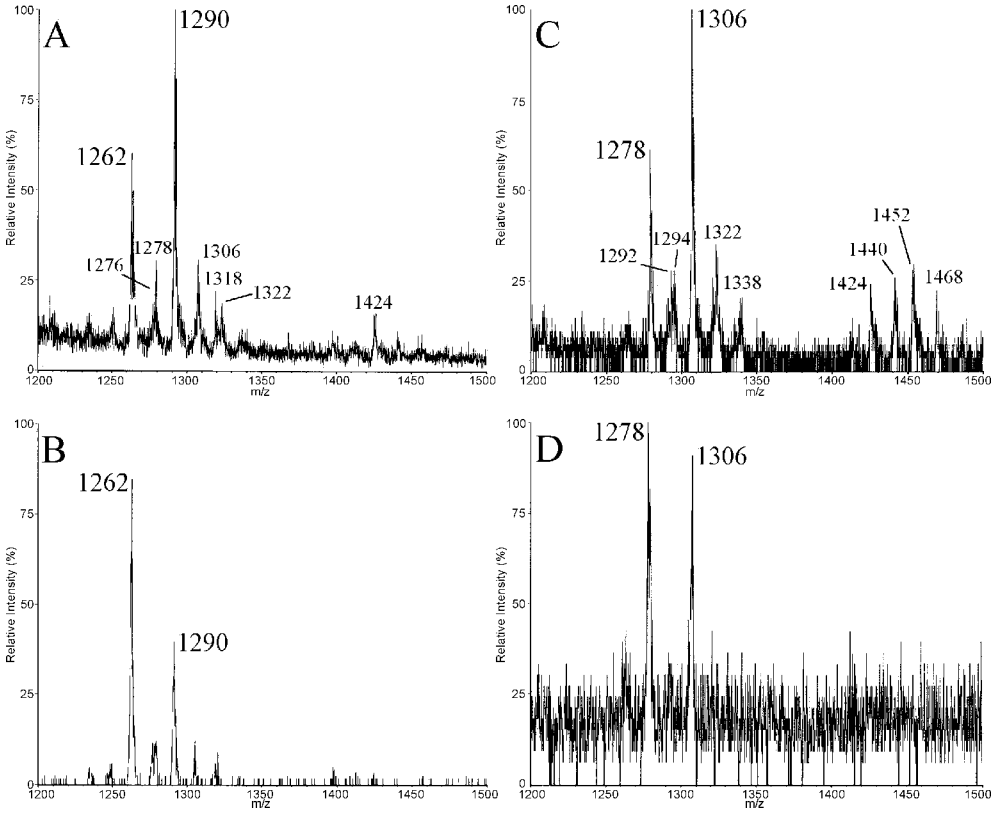

Figure 7. ESI-MS of M_2IPC from yeast form of *Sporothrix schenckii* (**Ss-Y1** and **Ss-Y2**). (A) Low OR Li^+ adduct profile of **Ss-Y1**; (B) corresponding Li^+ adduct precursor ion profile, acquired in tandem ESI-MS/CID-MS mode with selection of *m/z* 579 in Q3; (C) low OR Li^+ adduct profile of **Ss-Y2**; and (D) corresponding Li^+ adduct profile from precursor ion ESI-MS/CID-MS, with selection of *m/z* 579 in Q3.

sphingoid or fatty-N-acyl moiety. At high OR, fragments at *m/z* 255, 579 and 597, 741 and 759, and 690 were observed in the spectrum (not shown), respectively, corresponding to $[Ins\cdot P\cdot Li_2]^+$ ($[Y_1/B_3PO_3(Li)+Li]^+$), $[Hex_2\cdot Ins\cdot P\cdot Li_2]^+$ ($[Y_{2\alpha}$ or $Y_{2\beta}/B_3PO_3(Li)+Li]^+$ and $[Y_{2\alpha}$ or $Y_{2\beta}/C_3PO_3(Li)+Li]^+$), $[Hex_3\cdot Ins\cdot P\cdot Li_2]^+$ ($[B_3PO_3(Li)+Li]^+$ and $[C_3PO_3(Li)+Li]^+$), and $[Cer+Li]^+$ ($[Y_0+Li]^+$).

Tandem ESI-MS/CID-MS of this *m/z* 1424 component yielded a product spectrum (Fig. 10(A)) in which a full set of glycosylinositol and phosphorylglycosylinositol fragments can be observed (see Scheme 6, Table 3), i.e., pairs of fragments from phosphoryl and/or glycosidic cleavages at *m/z* 169 and 187 ($[B_1+Li]^+$ and $[C_1+Li]^+$), *m/z* 331 and 349 (from a variety of possible triple-cleavage ions), *m/z* 493 and 511 ($[B_2+Li]^+$ and $[C_2+Li]^+$), *m/z* 655 and 673 ($[B_3+Li]^+$ and $[C_3+Li]^+$), *m/z* 255 and 273 ($[Y_1/B_3PO_3(Li)+Li]^+$ and $[Y_1/C_3PO_3(Li)+Li]^+$), *m/z* 417 and 435 ($[Y_{2\alpha}/Y_{2\beta}/B_3PO_3(Li)+Li]^+$ and $[Y_{2\alpha}/Y_{2\beta}/C_3PO_3(Li)+Li]^+$), *m/z* 579 and 597 ($[Y_{2\alpha}$ or $Y_{2\beta}/B_3PO_3(Li)+Li]^+$ and $[Y_{2\alpha}$ or $Y_{2\beta}/C_3PO_3(Li)+Li]^+$), *m/z* 741 and 759 ($B_3PO_3(Li)+Li]^+$ and $C_3PO_3(Li)+Li]^+$), along with minor dehydration products at *m/z* 237 and 313. Particularly worth noting are the abundance ratios of the *m/z* 579/597 and 741/759 pairs, which are ~0.9:1 and ~0.5:1, respectively, with *m/z* 759 being overall the base peak. Based on our observations with simpler compounds, these ratios are consistent with the proposed Man$\alpha1\rightarrow2$Ins, rather than $1\rightarrow6$, linkage. The lineages are confirmed by ESI-$(CID\text{-}MS)^2$ with selection of *m/z* 759 and 741 (see later section). Another notable feature of the ESI-MS/CID-MS spectrum is the relatively low abundance of the *m/z* 417 and 435 pair. These represent fragments in which two glycosidic bonds are cleaved, a process which seems to be disfavored under these conditions, as was noted previously for ESI-MS/CID-MS of the Na^+ adduct of a branched GIPC from *Paracoccidioides brasiliensis*.[16] A ESI-MS/CID-MS spectrum of the *m/z* 1440 component yielded a product spectrum (not shown) which was of poorer quality, but essentially identical with respect to glycosylinositol and phosphorylglycosylinositol fragments.

With respect to the ceramide moiety of **Hc-M3a**, the $[Z_0PO_3(Li)+Li]^+$ expected at *m/z* 758 is overlapped by the $[C_3PO_3(Li)+Li]^+$ ion at *m/z* 759 (Fig. 10(A)), but $[Y_0+Li]^+$ and $[Y_0PO_3(Li)+Li]^+$ fragments at *m/z* 690 and 776, respectively, are observed; the accompanying $[O/Z_0PO_3(Li)+Li]^+$ at *m/z* 392 (with *m/z* 420 essentially absent) again indicates a fairly homogeneous t18:0/h24:0 composition for the major *m/z* 1424 component. In the ESI-MS/CID-MS of the *m/z* 1440 fraction, **Hc-M3b** (not shown), all fragments corresponding to the ceramide moiety were shifted by a +16 Th increment, in particular exhibiting an abundant $[Y_0+Li]^+$ fragment at *m/z* 706, as expected for the additional hydroxylation of this group. Since the $[O/Z_0PO_3(Li)+Li]^+$

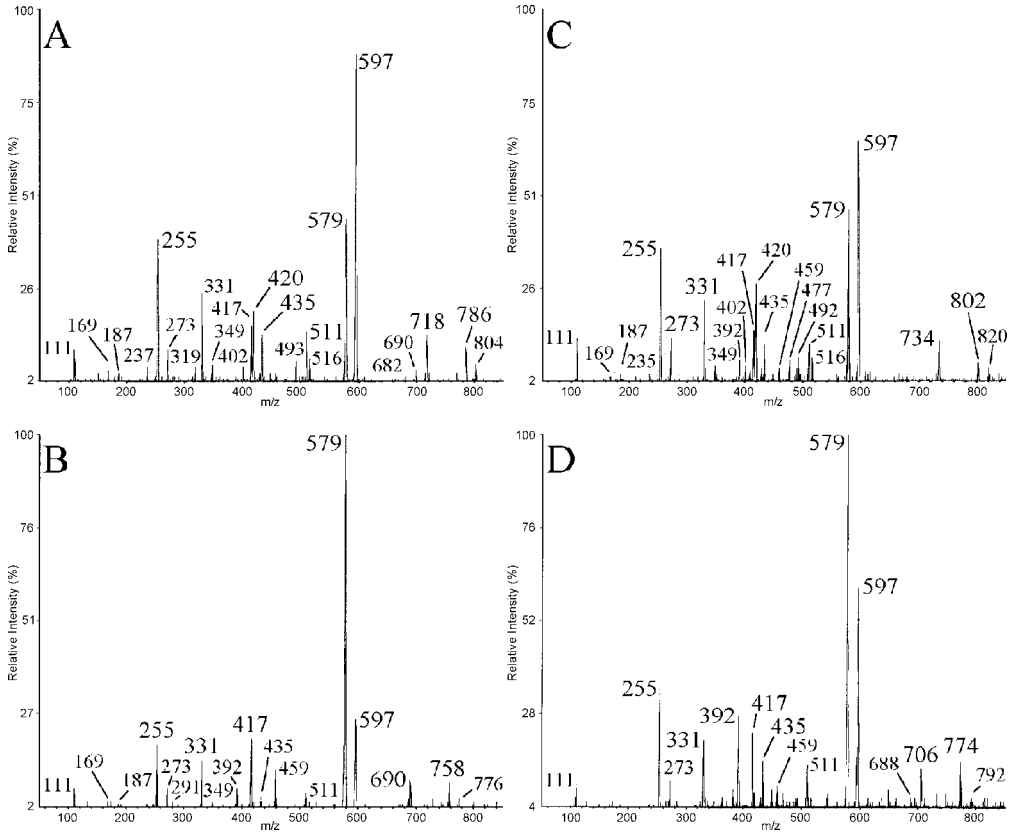

Figure 8. Tandem ESI-MS/CID-MS product ion spectra from $[M + Li]^+$ of M_2IPC from yeast form of *Sporothrix schenckii* (**Ss-Y1** and **Ss-Y2**). (A) Products of **Ss-Y1** $[M + Li]^+$ at *m/z* 1290; (B) products of **Ss-Y1** $[M + Li]^+$ at *m/z* 1262; (C) products of **Ss-Y2** $[M + Li]^+$ at *m/z* 1306; and (D) products of **Ss-Y2** $[M + Li]^+$ at *m/z* 1278.

ion was still observed at *m/z* 392, a fairly homogeneous t18:0 sphingoid composition is again indicated, with the extra hydroxyl group therefore confined to the fatty acid moiety (2h24:0). These conclusions, summarized in Table 2(A), could be confirmed by ESI-$(CID\text{-}MS)^2$ with selection of the major ceramide $[Y_0 + Li]^+$ fragments at *m/z* 690 or 706 (see later section).

The low OR single analyzer ESI-MS profile of the single *S. schenckii* mycelium fraction **Ss-M3** (Fig. 9(C)) was observed as a single major $[M + Li]^+$ at *m/z* 1424, similar to that of **Hc-M3a**. At high OR, the full spectrum (not shown) also exhibited essentially similar features to that of **Hc-M3a** as outlined above. Tandem ESI-MS/CID-MS scanning for precursors of the ions *m/z* 759 and 255 (not shown) confirmed that the only major molecular species in fraction **Ss-M3** giving rise to these products is the one observed at *m/z* 1424.

Tandem ESI-MS/CID-MS of this *m/z* 1424 component of **Ss-M3** yielded a spectrum (not shown) of glycosylinositol, phosphorylglycosylinositol, and ceramide-related fragments essentially indistinguishable from that of **Hc-M3a** (see Tables 2(A) and 3). The abundance ratios of the *m/z* 579/597 and 741/759 pairs were observed to be ~0.7:1 and ~0.5:1, respectively, consistent with the analysis of the **Hc-M3a** and its proposed Manα1 → 2Ins linkage. Observation of $[Y_0 + Li]^+$, $[Y_0PO_3(Li) + Li]^+$ and $[O/Z_0PO_3(Li) + Li]^+$ fragments at *m/z* 690, 776 and 392, respectively, again indicated a homogeneous t18:0/h24:0 ceramide composition for fraction **Ss-M3**, which was confirmed by ESI-$(CID\text{-}MS)^2$ with selection of the major ceramide $[Y_0 + Li]^+$ fragment at *m/z* 690 (see later section).

High OR tandem ESI-$(CID\text{-}MS)^2$ experiments

Glycosylphosphorylinositol ions

As a supplement to CID-MS of molecular adducts, CID-MS on fragments produced in the orifice-skimmer region of the ion source has a number of uses, including confirming the lineage for products observed in the molecular adduct spectra. The two examples shown in Figs 10(B) and 10(C) are high OR tandem ESI-$(CID\text{-}MS)^2$ of fraction **Hc-M3a**, with selection of glycosylphosphorylinositol ions (*m/z* 759 and 741, respectively) in Q1, and acquisition of CID product ion spectra in Q3. Under these conditions, secondary fragmentation of the glycosylphosphorylinositol primary ions was observed to be facilitated by Li^+ adduction compared with spectra of Na^+ adducts obtained under similar conditions (not shown). The product spectrum of $[C_3PO_3(Li) + Li]^+$, *m/z* 759 (Fig. 10(B)), exhibited essentially the same ions as the tandem ESI-MS/CID-MS of the $[M + Li]^+$ at *m/z* 1424 (Fig. 10(A)), but without any of the ceramide-related fragments (e.g., *m/z* 690 and 392). The abundance of the *m/z* 417 and 435 fragments ($[Y_{2\alpha}/Y_{2\beta}/B_3PO_3(Li) + Li]^+$ and $[Y_{2\alpha}/Y_{2\beta}/C_3PO_3(Li) + Li]^+$), in which two glycosidic bonds are cleaved, is again relatively low. Note that the product

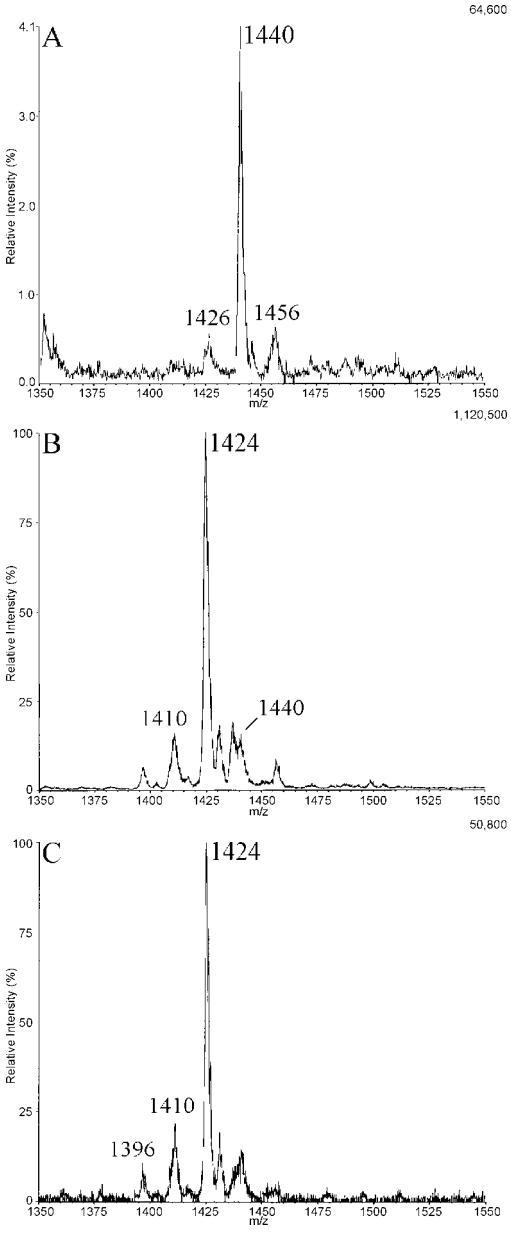

Figure 9. ESI-MS of $GalM_2IPC$ fractions from mycelium forms of *Histoplasma capsulatum* (**Hc-M3a, Hc-M3b**) and *Sporothrix schenckii* (**Ss-M3**). (A) Low OR Li^+ adduct profile of **Hc-M3b**; (B) low OR Li^+ adduct profile of **Hc-M3a**; and (C) low OR Li^+ adduct profile of **Ss-M3**.

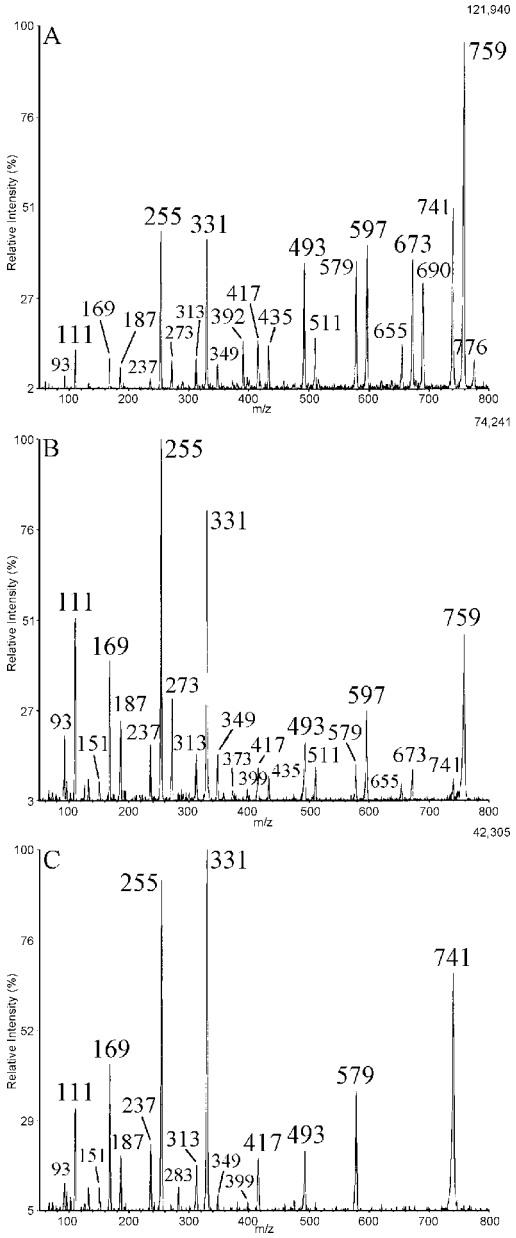

Figure 10. Tandem product ion spectra of lithiated $GalM_2IPC$ fraction from mycelium form of *Histoplasma capsulatum* (**Hc-M3a**). (A) Tandem ESI-MS/CID-MS product ion spectra from $[M + Li]^+$ at *m/z* 1424; (B) tandem ESI-CID-MS/CID-MS product ion spectra from primary phosphoglycan fragment $[C_3PO_3(Li) + Li]^+$ at *m/z* 759; and (C) tandem ESI-CID-MS/CID-MS product ion spectra from primary phosphoglycan fragment $[B_3PO_3(Li) + Li]^+$ at *m/z* 741.

spectrum of *m/z* 759 from **Ss-M3** (not shown) was virtually identical to that from **Hc-M3a**.

The product spectrum of $[B_3PO_3(Li) + Li]^+$, *m/z* 741 (Fig. 10(C)), exhibits further simplification, with the higher *m/z* member of each glycosidic cleavage pair deleted. Interestingly, the $[B_3 + Li]^+$ ion expected at *m/z* 655 is also entirely absent, suggesting that $[B_3PO_3(Li) + Li]^+$ takes the form of a cyclic phosphodiester, from which the phosphate would tend to resist being eliminated, and that the fragment *m/z* 493 therefore represents $[B_2 + Li]^+$ rather than $[Y_{2\alpha \text{ or } \beta}/B_3 + Li]^+$.

Ceramide ions

In other cases it is possible to detect from CID-MS of a primary fragment abundant product ions that are unobservable or of low abundance in the molecular adduct spectrum. For the GIPCs in this study it was found, for example, that CID-MS of ceramide $[Y_0 + Li]^+$ ions yielded several products whose appearance is otherwise marginal among the products of $[M + Li]^+$. This suggests in the latter case the presence of lower energy pathways proceeding via the phosphorylated ceramide ion, $[Z_0PO_3(Li) + Li]^+$ (i.e., decomposition of $[M + Li]^+$ to the primary $[Z_0PO_3(Li) + Li]^+$ fragment, followed by loss of the *N*-acyl chain to produce the $[O/Z_0PO_3(Li) + Li]^+$ fragment ion).

This difference is illustrated by ESI-$(CID\text{-}MS)^2$ product ion

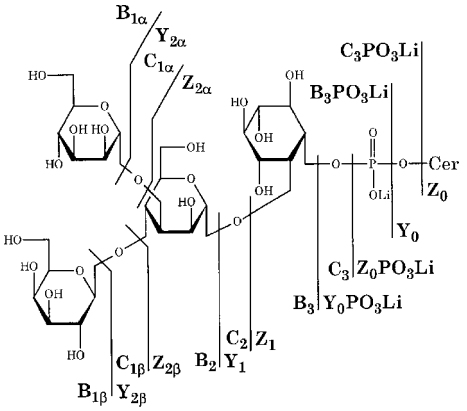

Scheme 6. Fragmentation of Mα3(Galβ4)Mα2IPC, with nomenclature according to Costello and Vath,[22] as modified for GIPCs.[40] Hydrogen transfers as in Schemes 2 and 3 are omitted here.

spectra with selection of the ceramide $[Y_0 + Li]^+$ fragments at *m/z* 718, 662 and 690 for the three major components in *A. blazei* fraction **Ab-1**, reproduced in Figs 11(A), (B), and (C), respectively. As with the ESI-(CID-MS)^2 of primary phosphoglycan ions discussed above, fragmentation of these $[Y_0 + Li]^+$ primary ions was observed to be facilitated by Li^+ adduction compared with spectra of Na^+ adducts obtained under similar conditions (not shown). The spectra are dominated by abundant phytosphingosine-derived N and $\underline{d}_{3b}$ fragments (*m/z* 352 and 319 for **Ab-1c**; *m/z* 324 and 291 for **Ab-1a**; a mixture of both pairs for **Ab-1b**). These fragments are of lower abundance or not observed at all in the ESI-MS/CID-MS product ion spectra of $[M + Li]^+$ precursors; nevertheless, they carry information related to the composition of the ceramide moiety, confirming the conclusions derived from the $[O/Z_0PO_3(Li) + Li]^+$ product ions discussed above. Lower abundance ions are assigned provisionally, as shown in Table 2(B). Conspicuously absent are W (acyl C_2-C_ω) ions,

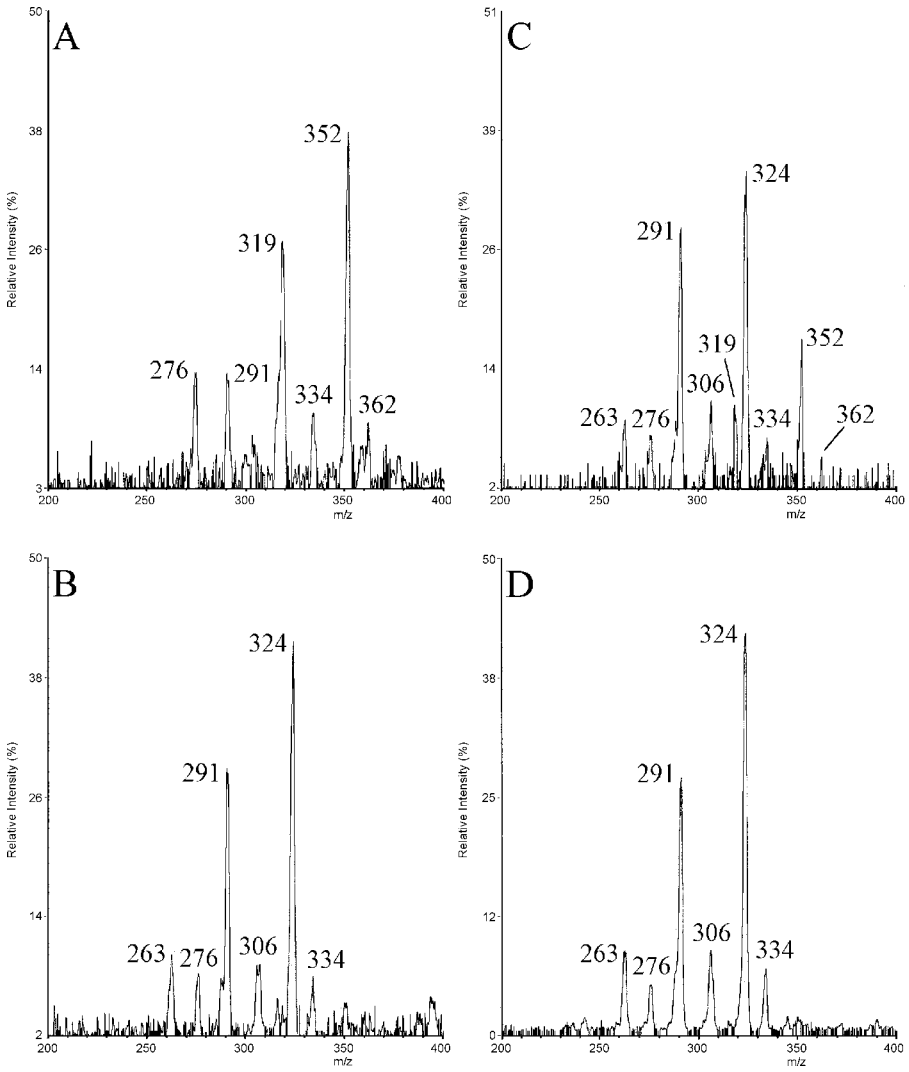

Figure 11. Expansions (*m/z* 200–400) of tandem ESI-CID-MS/CID-MS product ion spectra from $[Y_0 + Li]^+$ of GIPCs from *Agaricus blazei* (**Ab-1a,b,c**) and mycelium form of *Sporothrix schenckii* (**Ss-M1**). (A) Products of **Ab-1c** $[Y_0 + Li]^+$ at *m/z* 718; (B) products of **Ab-1a** $[Y_0 + Li]^+$ at *m/z* 662; (C) products of **Ab-1b(1 + 2)** $[Y_0 + Li]^+$ at *m/z* 690; and (D) products of **Ss-M1** $[Y_0 + Li]^+$ at *m/z* 690 (product spectra acquired for *m/z* 690 of **Ss-M2** and **Ss-M3** were essentially identical to this).

which have been observed previously in all CID spectra of lithiated GSLs having 2-hydroxy fatty-*N*-acylation;[28,30–33] this suggests that their appearance depends as well on the presence of an (*E*)-Δ^4 unsaturation in the ceramide sphingoid.

For the *S. schenckii* mycelium form fractions **Ss-M1-Ss-M3**, ESI-(CID-MS)^2 product ion spectra with selection of the common ceramide $[Y_0 + Li]^+$ ions at *m/z* 690 yielded essentially identical spectra, as exemplified by that for **Ss-M1** reproduced in Fig. 11(D). Products included abundant N and $\underline{d}_{3b}$ fragments at *m/z* 324 and 291; in contrast to the *m/z* 690 product ion spectrum for **Ab-1b** (cf. Fig. 11(C)), essentially no analogous *m/z* 352 or 319 fragments were detectable, eliminating the possibility of a contribution from t20:0/h22:0 components. A similar spectrum was obtained for the *H. capsulatum* mycelium fraction **Hc-M3a** (not shown).

In the case of the *S. schenckii* yeast form fraction **Ss-Y1**, ceramide $[Y_0 + Li]^+$ fragments arising from the two main components at *m/z* 718 (**Ss-Y1b**) and 690 (**Ss-Y1a**) yielded ESI-(CID-MS)^2 spectra exhibiting abundant N and $\underline{d}_{3b}$ pairs, at *m/z* 352 and 319 for the former, and at *m/z* 324 and 291 for the latter (Figs 12(A) and 12(B), respectively). These results confirm that the two components have the same h24:0 fatty-*N*-acyl moiety attached to two different phytosphingosines, t20:0 and t18:0, respectively. The corresponding components of **Ss-Y2**, proposed to have an analogous pair of ceramides with dihydroxy fatty-*N*-acylation, exhibited ceramide $[Y_0 + Li]^+$ fragments in ESI-CID-MS or ESI-MS/CID-MS spectra at *m/z* 734 (**Ss-Y2b**) and 706 (**Ss-Y2a**), respectively. Similar to the **Ss-Y1** components, ESI-(CID-MS)^2 spectra of these **Ss-Y2** $[Y_0 + Li]^+$ fragments again exhibited N and $\underline{d}_{3b}$ pairs, at *m/z* 352 and 319 for the former, and at *m/z* 324 and 291 for the latter (Figs 12(C) and 12(D), respectively); interestingly, however, in both spectra of these dihydroxy fatty-*N*-acylated species the N ion was superabundant, appearing at intensities 4–5 times that of the $\underline{d}_{3b}$ ion, contrasting with N/$\underline{d}_{3b}$ ratios that are <2 in all cases with monohydroxy fatty-*N*-acylated ceramides. This suggests a substantially increased activation of the de-*N*-acylation

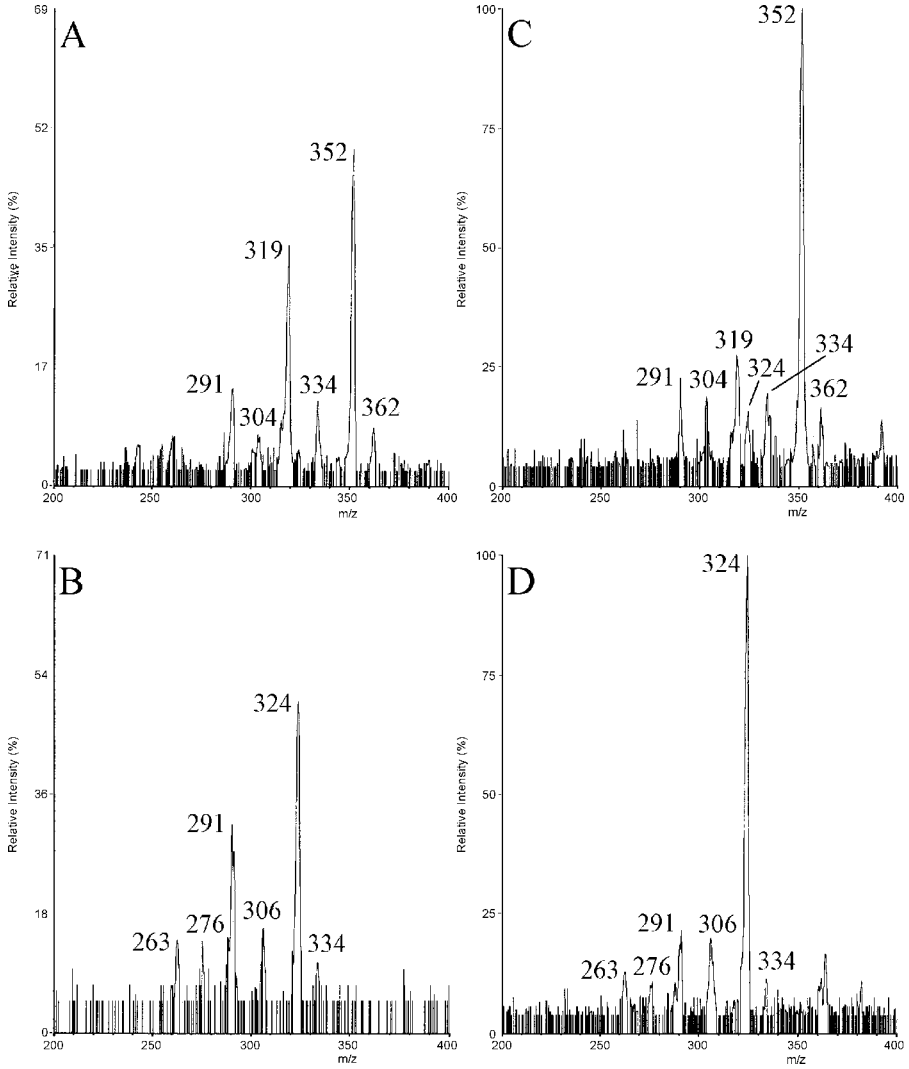

Figure 12. Expansions (*m/z* 200–400) of tandem ESI-CID-MS/CID-MS product ion spectra from $[Y_0 + Li]^+$ of GIPCs from yeast form of *Sporothrix schenckii* (**Ss-Y1** and **Ss-Y2**). (A) Products of **Ss-Y1b** $[Y_0 + Li]^+$ at *m/z* 718; (B) products of **Ss-Y1a** $[Y_0 + Li]^+$ at *m/z* 690; (C) products of **Ss-Y2b** $[Y_0 + Li]^+$ at *m/z* 734; and (D) products of **Ss-Y2a** $[Y_0 + Li]^+$ at *m/z* 706.

reaction under these conditions by the additional hydroxy group. A low-abundance ion, *m/z* 324, in the spectrum of the *m/z* 734 component (**Ss-Y2b**; Fig. 12(C)) corresponds to a trace amount of t18:0/2h26:0 species (**Ss-Y2b2**) along with the major t20:0/2h24:0 component (**Ss-Y2b1**).

An ESI-(CID-MS)^2 spectrum similar to that for *m/z* 706 of **Ss-M3a** was obtained for the same primary $[Y_0 + Li]^+$ fragment of *H. capsulatum* mycelium component **Hc-M3b** (not shown). Results for all ESI-(CID-MS)^2 of $[Y_0 + Li]^+$ fragments are summarized in Table 2(B).

DISCUSSION

As observed previously with cerebrosides[17,31-33] and complex neutral glycosphingolipids,[33] the use of Li^+ cationization with tandem quadrupole ESI-MS/CID-MS of glycosylinositol phosphorylceramides yielded a substantial increase in observable fragmentation compared with spectra obtained from sodiated species acquired under comparable conditions. However, GIPCs differ from these other types of glycosphingolipids in a number of respects, and the differences are reflected in some general features of their fragmentation spectra. Key structural differences include (i) interpolation of *myo*-inositol-1-phosphate between ceramide and glycan, which introduces both anionic character and a non-glycosidic residue at the oligosaccharide reducing end; and (ii) the predominance of saturated, polyhydroxylated ceramides (phytoceramides), rather than those containing an (*E*)-Δ^4-unsaturated sphingoid, for example, as commonly found in both mammalian glycosphingolipids and in the cerebrosides of fungi and plants (in the latter two cases predominantly accompanied by Δ^8 unsaturation as well). In mammals, glycosphingolipids with 4-hydroxysphinganine (phytosphingosine) are found, but with limited tissue/cell-type distribution patterns.[1] Likewise, 2-hydroxy fatty-*N*-acylated species are also found in some mammalian tissues; for example, they make up almost half of the ceramides of galactocerebroside, galactosulfatide, and G_{M4} ganglioside expressed in brain and peripheral nerve, but in combination with sphing-4-enines. Ceramides containing both phytosphingosine and 2-hydroxy fatty-*N*-acylation are found in some glycosphingolipids from mammalian kidney and stomach, in Lewis-type antigens found as minor, non-endogenous components of erythrocytes, and in antigens characteristic of certain cancers. In general, GIPCs are not found in higher animals, but are characteristic glycosphingolipid components of fungi and plants.[3]

Previously, native GIPCs have been analyzed by other ESI-MS protocols, including profiling molecular ion species in negative ion mode as $[M - H]^-$ or by parent ion scanning from *m/z* 79 for phosphate anion;[17] in the same work, negative ion mode ESI-MS/CID-MS was used to obtain glycosylphosphorylinositol ions and glycosidic fragments thereof, as well as ceramide phosphate ions. No attempt was made to compare directly the relative merits of the negative ion detected methods described by Jennemann *et al.*[17] to those in the current study.

It is worth noting that other types of phospholipids, including sphingomyelins, have been analyzed using Li^+ adduction with ESI-MS and ESI-MS/CID-MS,[42,43] but extension of the methodology to GIPCs involves a number of additional considerations due to the extensive variability and complexity of the glycosylinositol headgroups, as well as to the differences in fragmentation manifested by phytoceramides versus diacylglycerols, alkylacylglycerols, or the (*E*)-Δ^4-unsaturated ceramide found predominantly in mammalian sphingomyelins. Under conditions of low-energy CID, fragmentations of the ceramides or phosphorylceramides containing a phytosphingosine moiety appear to be rather limited in comparison to those having sphing-4-enines or sphing-4,8-dienines. On the other hand, in common with other ceramides containing 2-hydroxy fatty-*N*-acylation, loss of the amide-linked fatty acid moiety (O) is retained as a significant fragmentation mode. Interestingly, the abundance of this fragment was increased by additional hydroxylation of the fatty acid. In the absence of (*E*)-Δ^4 unsaturation of the sphingoid, fragments that involve cleavage of the sphingoid C2–C3 bond (G, T [$\equiv$Z0/G]) are not observed. Another fragment, particularly characteristic of the 2-hydroxy fatty acid moiety (W, i.e., cleavage of the acyl C2–C3 bond to produce a long chain aldehyde), was also not observed. We found this somewhat surprising, since the reason for dependence of this cleavage on the presence of sphingoid (*E*)-Δ^4 unsaturation does not appear to be obvious. It does suggest that, perhaps, it does not follow directly after generation of a ceramide ion, but mainly occurs after other fragmentations of ceramide, dependent on the (*E*)-Δ^4 unsaturation, have taken place (compare pathways in Scheme 4 of Hsu and Turk[33]).

In any case, sufficient information for establishing the absolute lengths of the alkyl and acyl chains, as well as the number of hydroxyl groups disposed on each, in a phytoceramide is still conveniently available from tandem MS/CID-MS experiments; for the former purpose in particular, NMR spectroscopy is not very useful, since the bulk of mid-chain alkyl/acyl CH_2 groups resonate at a single frequency. The current study has disclosed a fairly narrow range of differences in the distribution of each of these ceramide structural elements, but within these limitations it appeared that all possible combinations are utilized, and used differently in each fungus examined, or in some cases differed even between one GIPC and another in the same fungus. These observations suggest that rather strict cellular controls are exercised in GIPC ceramide biosynthesis.

With respect to glycosylinositol fragmentation, the persistence of sets of ions retaining the phosphate provides a useful marker for the reducing end of the glycan. We observed mainly glycosidic cleavages, with the possibilities of bond breakage on either side of the glycosidic oxygen, Li^+ retention on either the reducing or non-reducing portion of the glycan, and retention or loss of lithium phosphate. The apparent variance in abundance ratios for the primary phosphorylglycosylinositol ($[B_nPO_3(Li) + Li]^+$ and $[C_nPO_3(Li) + Li]^+$) ions depending on the linkage of Man to Ins (Manα1 $\rightarrow$ 6Ins versus Manα1 $\rightarrow$ 2Ins) should prove to be useful in structural characterization, but it would be desirable to test GIPCs with other core glycosidic linkages (i.e., Manα1 $\rightarrow$ 3Ins, 1 $\rightarrow$ 4Ins, 1 $\rightarrow$ 5Ins) to observe their effects. GIPCs with Manα1 $\rightarrow$ 4Ins have been reported in basidiomycetes,[17] but have not yet been isolated in pure form.

Considering that in both Man$\alpha1 \rightarrow 6$Ins and Man$\alpha1 \rightarrow 2$Ins compounds the Man residues are attached to hydroxyl groups adjacent to the phosphoryl ester group (at O-1 of *myo*-inositol), this must be related mainly to the difference in configuration at C-2 versus C-6 of the *myo*-inositol residue (the hydroxyl group is oriented axially at C-2, equatorially at C-6). It is not yet clear in this case whether *m/z* 417 is simply a product of dehydration of *m/z* 435, or if the ions are both primary products of cleavage processes occurring on either side the Cer O-1 atom. The difference could in either case be related to the ability of the phosphorylglycosylinositol moiety to form a cyclic phosphate at O-2 or O-6 when the other hydroxyl group not available. One might expect that the 1,2- would be more difficult to form than the 1,6-cyclic phosphate, since the former involves O-atoms in equatorial-axial relationship, while in the latter they are both equatorial. If this were the case, it would then imply that the cyclization to $[B_2PO_3(Li) + Li]^+$ should occur more readily for Man-$\alpha1 \rightarrow 2$Ins-P than for Man$\alpha1 \rightarrow 6$Ins-P, but the opposite appears to be the case. It is possible that the Li^+ somehow activates the cyclization of phosphate in a way that is more favorable for the 1,2-case, but it is difficult to envision how.

It is expected that the methodology described will be applicable for studies of more complex GIPCs from fungi, and can be adapted to instrument configurations providing more rapid and sensitive analysis. It should be emphasized that, since isobaric molecular species can be produced by variations of both glycan and ceramide features, as illustrated by several cases in the present study, the use of product ion mode tandem CID experiments is an essential element of a GIPC structural elucidation strategy based on mass spectrometry. With crude lipid mixtures, profiling GIPC molecular species by scanning for precursors of a single common product ion in a triple quadrupole instrument[44] may be useful, but in most cases will be insufficient for either qualitative or quantitative analysis. Some form of prior fractionation is desirable, and, ideally, mixture analysis would be performed via a direct HPLC interface, using a more sensitive state-of-the-art instrument designed for rapid scanning and automated acquisition of CID spectra.

Acknowledgements

This work was supported by FAPESP, CNPq, and PRONEX (Brasil; M.S.T., A.H.S., and H.K.T.); a Glycoscience Research Award from Neose Technologies, Inc. (S.B.L.); and the National Institutes of Health Resource Center for Biomedical Complex Carbohydrates (NIH #5 P41 RR05351; S.B.L.).

REFERENCES

1. Kanfer JN, Hakomori S. *Sphingolipid Biochemistry*, Plenum Press: New York, 1983.
2. Dickson RC. *Ann. Rev. Biochem.* 1998; **67**: 27.
3. Lester RL, Dickson RC. *Adv. Lipid Res.* 1993; **26**: 253.
4. Nagiec MM, Nagiec EE, Baltisberger JA, Wells GB, Lester RL, Dickson RC. *J. Biol. Chem.* 1997; **272**: 9809.
5. Dickson RC, Lester RL. *Biochim. Biophys. Acta* 1999; **1426**: 347.
6. Daum G, Lees ND, Bard M, Dickson R. *Yeast* 1998; **14**: 1471.
7. Takesako K, Kuroda H, Inoue T, Haruna F, Yoshikawa Y; Kato I. *J. Antibiot.* 1993; **49**: 1414.
8. Mandala SM, Thornton RA, Rosenbach M, Milligan J, Garcia-Calvo M, Bull HG, Kurtz MB. *J. Biol. Chem.* 1997; **272**: 32709.
9. Mandala SM, Thornton RA, Milligan J, Rosenbach M, Garcia-Calvo M, Bull HG, Harris G, Abruzzo GK, Flattery AM, Gill CJ, Bartizal S, Kurtz MB. *J. Biol. Chem.* 1998; **273**: 14942.
10. Zhong W, Jeffries MW, Georgopapadakou NH. *Antimicrob. Agents Chemother.* 2000; **44**: 651.
11. Georgopapadakou NH. *Expert Opin. Investig. Drugs* 2000; **9**: 1787.
12. Barr K, Lester RL. *Biochemistry* 1984; **23**: 5581.
13. Barr K, Laine RA, Lester RL. *Biochemistry* 1984; **23**: 5589.
14. Toledo MS, Suzuki E, Straus AH, Takahashi HK. *J. Med. Vet. Mycol.* 1995; **33**: 247.
15. Jennemann R, Bauer BL, Bertalanffy H, Selmer T, Wiegandt H. *Immunobiology* 1999; **200**: 277.
16. Levery SB, Toledo MS, Straus AH, Takahashi HK. *Biochemistry* 1998; **37**: 8764.
17. Jennemann R, Geyer R, Sandhoff R, Gschwind RM, Levery SB, Gröne H-J, Wiegandt H. *Eur. J. Biochem.* 2001; **268**: 1190.
18. Toledo MS, Levery SB, Straus AH, Takahashi HK. *FEBS Lett.* 2001; **493**: 50.
19. Toledo MS, Levery SB, Glushka J, Straus AH, Takahashi HK. *Biochem. Biophys. Res. Commun.* 2001; **280**: 19.
20. Dell A. *Adv. Carbohydr. Chem. Biochem.* 1987; **45**: 19.
21. Egge H, Peter-Katalinic J. *Mass Spectrom. Rev.* 1987; **6**: 331.
22. Costello CE, Vath JE. *Methods Enzymol.* 1990; **193**: 738.
23. Adams J, Ann Q. *Mass Spectrom. Rev.* 1993; **12**: 51.
24. Peter-Katalinic J. *Mass Spectrom. Rev.* 1994; **13**: 77.
25. Ann Q, Adams J. *J. Am. Soc. Mass Spectrom.* 1992; **3**: 260.
26. Ann Q, Adams J. *Anal. Chem.* 1993; **65**: 7.
27. Duarte RS, Polycarpo CR, Wait R, Hartmann R, Bergter EB. *Biochim. Biophys. Acta* 1998; **1390**: 186.
28. Sullards MC, Lynch DV, Merrill AHJ, Adams J. *J. Mass Spectrom.* 2000; **35**: 347.
29. Pocsfalvi G, Malorni A, Mancini I, Guella G, Pietra F. *Rapid. Commun. Mass. Spectrom.* 2000; **14**: 2247.
30. Olling A, Breimer ME, Samuelsson BE, Ghardashkhani S. *Rapid. Commun. Mass Spectrom.* 1998; **12**: 637.
31. Levery SB, Toledo MS, Straus AH, Takahashi HK. *Rapid. Commun. Mass Spectrom.* 2000; **14**: 551.
32. Toledo MS, Levery SB, Suzuki E, Straus AH, Takahashi HK. *Glycobiology* 2001; **11**: 113.
33. Hsu F-F, Turk J. *J. Am. Soc. Mass Spectrom.* 2001; **12**: 61.
34. Levery SB, Toledo MS, Doong RL, Fuller M, Straus AH, Takahashi HK. *Proc. 48th ASMS Conf. Mass Spectrometry Allied Topics*, 2000, Abstract.
35. Levery SB, Toledo MS, Doong RL, Fuller M, Straus AH, Takahashi HK. *Proc. 49th ASMS Conf. Mass Spectrometry Allied Topics*, 2001, Abstract.
36. Toledo MS, Levery SB, Straus AH, Takahashi HK. *J. Lipid Res.* 2000; **41**: 797.
37. Toledo MS, Levery SB, Straus AH, Suzuki E, Momany M, Glushka J, Moulton JM, Takahashi HK. *Biochemistry* 1999; **38**: 7294.
38. Domon B, Vath JE, Costello CE. *Anal. Biochem.* 1990; **184**: 151.
39. Domon B, Costello CE. *Biochemistry* 1988; **27**: 1534.
40. Singh BN, Costello CE, Beach DH. *Arch. Biochem. Biophys.* 1991; **286**: 409.
41. Metelmann W, Muthing J, Peter-Katalinic J. *Rapid. Commun. Mass Spectrom.* 2000; **14**: 543.
42. Hsu FF, Turk J. *J. Mass. Spectrom.* 2000; **35**: 595.
43. Hsu FF, Turk J. *J. Am. Soc. Mass. Spectrom.* 2000; **11**: 437.
44. Gu M, Kerwin JL, Watts JD, Aebersold R. *Anal. Biochem.* 1997; **244**: 347.
45. Domon B, Costello CE. *Glycoconj. J.* 1988; **5**: 397.
46. Assam MR, Glish GL. *J. Am. Soc. Mass Spectrom.* 1997; **8**: 987.